SUBJECT-SPECIFIC FINITE ELEMENT PREDICTIONS OF KNEE CARTILAGE PRESSURE AND INVESTIGATION OF CARTILAGE MATERIAL MODELS

A Thesis

presented to

the Faculty of California Polytechnic State University,

San Luis Obispo

In Partial Fulfillment

of the Requirements for the Degree

Master of Science in Mechanical Engineering

by

Michael Gertmenian Rumery

September 2018

COMMITTEE MEMBERSHIP

TITLE: SUBJECT-SPECIFIC FINITE ELEMENT PREDICTIONS OF KNEE CARTILAGE PRESSURE AND INVESTIGATION OF CARTILAGE MATERIAL MODELS

AUTHOR: Michael Gertmenian Rumery

DATE SUBMITTED: September 2018

COMMITTEE CHAIR: Scott Hazelwood, Ph.D.
Professor of Biomedical Engineering

COMMITTEE MEMBER: Stephen Klisch, Ph.D.
Professor of Mechanical Engineering

COMMITTEE MEMBER: Joseph Mello, Ph.D.
Professor of Mechanical Engineering

ABSTRACT

SUBJECT-SPECIFIC FINITE ELEMENT PREDICTIONS OF KNEE CARTILAGE PRESSURE AND INVESTIGATION OF CARTILAGE MATERIAL MODELS

Michael Gertmenian Rumery

An estimated 27 million Americans suffer from osteoarthritis (OA). Symptomatic OA is often treated with total knee replacement, a procedure which is expected to increase in number by 673% from 2005 to 2030, and costs to perform total knee replacement surgeries exceeded $11 billion in 2005. Subject-specific modeling and finite element (FE) predictions are state-of-the-art computational methods for anatomically accurate predictions of joint tissue loads in surgical-planning and rehabilitation. Knee joint FE models have been used to predict in-vivo joint kinematics, loads, stresses and strains, and joint contact area and pressure. Abnormal cartilage contact pressure is considered a risk factor for incidence and progression of OA. For this study, three subject-specific tibiofemoral knee FE models containing accurate geometry were developed from magnetic resonance images (MRIs). Linear (LIN), Neo-Hookean (NH), and poroelastic (PE) cartilage material models were implemented in each FE model for each subject under three loading cases to compare cartilage contact pressure predictions at each load case. An additional objective was to compare FE predictions of cartilage contact pressure for LIN, NH, and PE material models with experimental measurements of cartilage contact pressure. Because past studies on FE predictions of cartilage contact pressure using different material models and material property values have found differences in cartilage contact

pressure, it was hypothesized that different FE predictions of cartilage contact pressure using LIN, NH, and PE material models for three subjects at three different loading cases would find statistically significant differences in cartilage contact pressure between the material models. It was further hypothesized that FE predictions of cartilage contact pressure for the PE cartilage material model would be statistically similar to experimental data, while the LIN and NH cartilage material models would be significantly different for all three loading cases. This study found FE and experimental measurements of cartilage contact pressure only showed significant statistical differences for LIN, NH, and PE predictions in the medial compartment at 1000N applied at 30 degrees, and for the PE prediction in the medial compartment at 500N applied at 0 degrees. FE predictions of cartilage contact pressure using the PE cartilage material model were considered less similar to experimental data than the LIN and NH cartilage material models. This is the first study to use LIN, NH, and PE material models to examine knee cartilage contact pressure predictions using FE methods for multiple subjects and multiple load cases. The results demonstrated that future subject specific knee joint FE studies would be advised to select LIN and NH cartilage material models for the purpose of making FE predictions of cartilage contact pressure.

ACKNOWLEDGMENTS

Thank you to Dr. Scott Hazelwood and Dr. Stephen Klisch for their commitment to our HMB lab and student success in research. Your advice and guidance has been phenomenal and will be appreciated for years to come.

Thank you to my HMB Lab family: In particular my outstanding thesis partner Greg Lane, Greg Orekhov, Jordan, Sam, Eshan, Katherine, Megan, Gabe and every student who has shared time working in the lab together.

Thank you to David Tuttle M.D., Paul Flaherty, and Carol Reynders of Radiology at French Hospital in San Luis Obispo for performing our MRIs.

Thank you to students and professors from CE 204, CE 207, ME 326, ME 404, and ME 503 labs and activities. The kindness and knowledge you have shared with me in our many experiences has forever changed me for the better.

Thank you to my wonderful family: Mom, Pops, big sisters Jen and Kristin and Vuh-Vuh, brothers-in-laws Evan and James, my Nana and Gar, my Aunts and Uncle, Cousins, and longtime family-like friends from Davis, CA: Sammy T, Ryles, Andy, Jacob, Benjy, M10, Barnes, bMac, Buckley, G Hos, and CQ. The interest, care, and support you have given me is more than anyone could ask for.

Thank you to wonderful Emma, voice of reason and biggest source of joy.

This work was supported by the Defense Health Program, through the Department of Defense Broad Agency Announcement for Extramural Medical Research Program Number W81XWH-BAA-14-1 under Award No. W81XWH-16-1-0051. Opinions, interpretations, conclusions and recommendations are those of the author and are not necessarily endorsed by the Department of Defense.

TABLE OF CONTENTS

LIST OF TABLES

LIST OF FIGURES

Figure Page

CHAPTER 1

INTRODUCTION

Osteoarthritis (OA) is one of the four major musculoskeletal conditions, in addition to osteoporosis, rheumatoid arthritis, and low back pain [1], and worldwide an estimated 9.6% of men and 18.0% of women over 60 years old have symptomatic OA [2]. A global study found that the prevalence of hip and knee OA was the 11th highest contributor to global disability of 291 conditions considered [3]. In the United States, OA affects 13.9% of adults aged 25 and older, and 33.6% over the age of 65; an estimated 27 million Americans total suffer from OA [4]. Symptomatic OA of the knee is often treated with total knee replacement, a procedure performed 615,000 times in the United States in 2008, a number of procedures that has more than doubled since 1999 [5]. From 2005 to 2030 the demand for total knee replacements is projected to grow by 673% [6]. The cost to perform total knee replacements in the United States in 2005 exceeded $11 billion [7].

Subject-specific finite element (FE) predictions are state-of-the-art computational methods for anatomically accurate predictions of joint tissue loads [8, 9]. Surgical and rehabilitation studies have utilized FE predictions of knee joint biomechanics to investigate risk factors for incidence and progression of OA [10–22]. Past studies have reported extensively on kinematics, principal stress and strain, von Mises stress, contact area and contact pressure results. The majority of past studies have investigated the tibiofemoral joint [10–16, 18–21], while some studies have included only the patellofemoral joint [23–30], and other

studies have included tibiofemoral and patellofemoral joints simultaneously [17, 22]. Past knee joint finite element models have been used to investigate the effects of osteochondral defects [11, 15], focal cartilage defects [16, 17], total knee replacement [31, 32], meniscectomy [18–22], and ACL deficiency [25, 33] on knee joint biomechanics.

The effects of cartilage material model choices have been investigated in past studies for FE predictions using linear (LIN), Neo-Hookean (NH), poroelastic (PE), transversely isotropic poroelastic (TIPE), depth-dependent, and fibril-reinforced poroelastic (FRPE) material models [34–41]. A study on FE predictions using a LIN cartilage material model found cartilage contact pressure increased by 56.6% and 24.0% on the tibial and femoral surfaces, respectively, when modulus was increased from 5 MPa to 20 MPa [40]. A study found that during 25% stance phase of gait LIN predictions of cartilage contact pressure were 19% and 30% less for mean and peak pressure, respectively, compared to FE predictions using a depth-dependent fibril-reinforced cartilage material model [41]. A study comparing FE predictions for LIN, PE, TIPE, and FRPE cartilage material models determined that it was not possible to specify material parameter values that simultaneously predicted the same cartilage contact pressure and principal stress across material models [34].

Investigating the effects of material model choice for FE predictions of knee cartilage contact pressure is desired because abnormal cartilage contact pressure is considered a risk factor for OA [42]. No past studies investigating the effects of different cartilage material models on FE predictions have clearly

reported cartilage contact pressures for multiple homogenous isotropic cartilage material models such as LIN, NH, and PE in the same study. In addition all past studies on the effects of cartilage material models on FE predictions of tibiofemoral joint biomechanics have been limited to one subject [34–41]. A study comparing FE predictions of cartilage contact pressure for multiple subjects at multiple loads would be the first study to determine if significant differences in FE predictions for LIN, NH, and PE cartilage material models exist. The LIN, NH, and PE cartilage material models have been selected for this study specifically because isotropic homogenous material models are the most feasible and straightforward to implement and nonhomogeneous fibril reinforced models are considerably more difficult to implement. The PE cartilage material model was selected because past studies found that including the effects of voids was important to accurately capture the mechanical response of cartilage [34]. In order for subject-specific tibiofemoral joint knee modeling to become more widely used to make decisions in surgical planning and rehabilitation, it is necessary for the material modeling processes to be made as simple and consistently repeatable as possible.

The objective of this study was to develop three subject-specific tibiofemoral knee FE models and compare FE predictions of cartilage contact pressure using LIN, NH, and PE cartilage material models at three different loading cases. An additional objective was to compare FE predictions of cartilage contact pressure for LIN, NH, and PE material models with experimental measurements of cartilage contact pressure in order to attempt to determine

which material model may best match experimental results in FE simulations of tibiofemoral knee models. Because past studies on FE predictions of cartilage contact pressure using different material models and material property values have found differences in cartilage contact pressure, it was hypothesized that different FE predictions of cartilage contact pressure using LIN, NH, and PE material models for three subjects at three different loading cases will find statistically significant differences in cartilage contact pressure between material models. This study also asserted as a hypothesis that FE predictions of cartilage contact pressure for the PE cartilage material model will be statistically similar to experimental data while the LIN and NH cartilage material models will be significantly different for all three loading cases.

CHAPTER 2

METHODS

This section provides relevant procedures for performing the analyses used in this study. Further information on the methods, including more details on the model development, are provided in Appendix E.

Participant Information

Three healthy, young male adults volunteered for this study. Participant demographics are presented in Table 2.1. The three participants were admissible within the eligibility criteria as approved by IRB protocol of the magnetic resonance imaging (MRI) procedure. Participants had no known knee injuries.

Table 2.1: Participant demographics and measurements.

Subject ID	Dominant Leg	Gender	Age [Yrs]	Height [m]	BMI [kg/m^2]
1	Right	Male	21	1.82	25.0
2	Left	Male	23	1.75	28.9
3	Right	Male	22	1.79	19.1

MRI Procedure

The MRIs were performed at a local, non-research hospital due to its proximity to our motion analysis lab. The protocol was approved by Cal Poly's Human Subjects Committee and designed to minimize risks to participants. Care was taken to ensure the entire MRI appointment was less than 60 minutes in total to minimize movement artifacts and participant discomfort. The MRIs were performed on a GE Signa HDxt 1.5T scanner (GE Healthcare, Little Chalfont,

UK). The optimal sequence for best identifying knee tissues using this machine was determined to be a proton density fast spin-echo, fat saturated sequence (4800 second relaxation time, 32.1 second echo time, 2 averages, 90-degree flip angle) in the sagittal plane with 1 mm slice thickness and a 512x512 matrix. The MRIs were evaluated by a board certified radiologist and were approved for use as healthy subjects for this study.

Geometry and Mesh Generation

Three subject-specific knee models were created from MRIs. Finalized three-dimensional knee models contained the bones, cartilage, menisci, and ligaments of the tibiofemoral joint with a sufficiently high-quality mesh for accurate finite element analysis. Image segmentation was performed using manual segmentation tools utilized in ITK-SNAP (University of Pennsylvania, Philadelphia, PA, USA) [43], with bone, menisci, and cartilage outlined as shown in Figure 2.1. Surface processing including cleaning, smoothing, and remeshing 3-D surfaces was performed in MeshLab (Institute for Computer Science and Technologies, Pisa, Italy) [44] for bone, cartilage, and menisci. Quadratic tetrahedral meshes for the cartilage and menisci were created using TetGen (Weierstrass Institute for Applied Analysis and Stochastics, Berlin, Germany) [45]. The surfaces of the bones and tetrahedral meshes of the cartilage and menisci were combined to form a tibiofemoral knee joint assembly in Abaqus (Dassault Systems, Providence, Rhode Island, USA) shown in Figure 2.2 using

custom-written scripts and the GIBBON[54] toolbox for MATLAB (MathWorks, Natick, Massachusetts, USA).

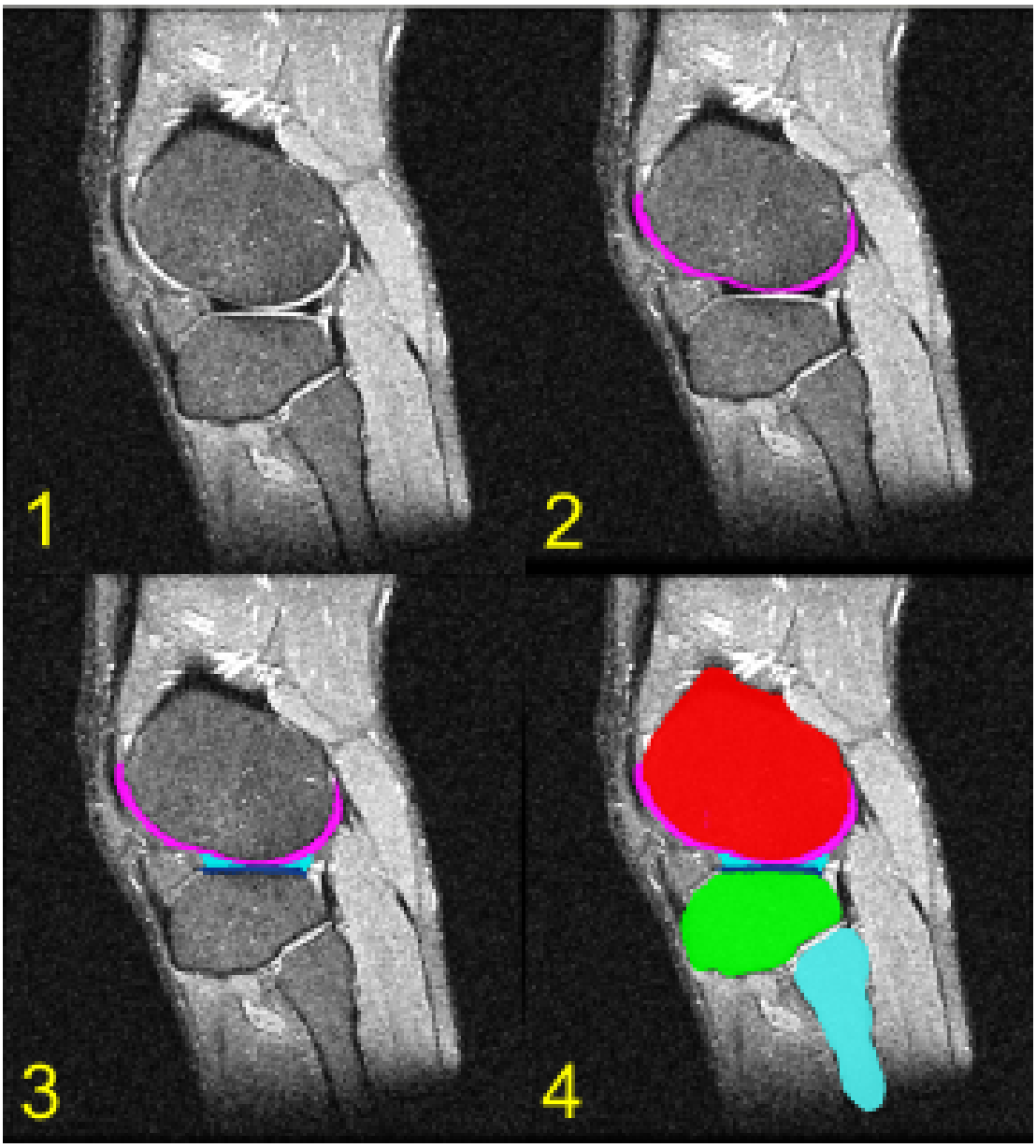

Figure 2.1: Femur (red), Tibia (green), Fibula (teal), femoral cartilage (pink), tibial cartilage (blue), menisci (aqua), were outlined in ITK-SNAP.

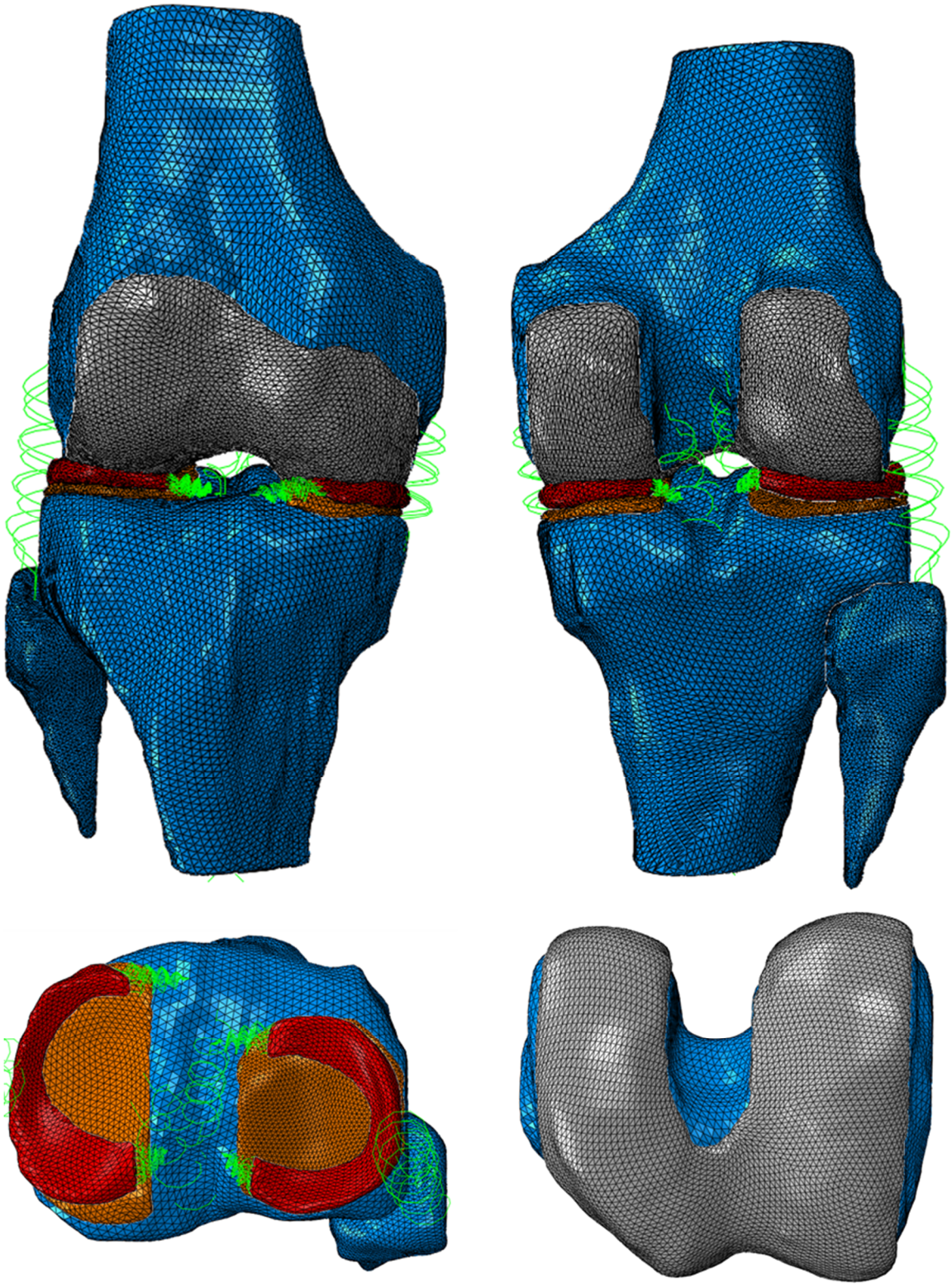

Figure 2.2: Subject 01 knee mesh assembly showing bones in blue, femoral cartilage in gray, tibial cartilage in orange, menisci in red, and ligaments and meniscal attachments in bright green.

Constitutive Modeling

FE predictions in this study were made using LIN, NH, and PE cartilage material models with the properties shown in Table 2.2. The uniaxial responses of LIN, NH, and PE material models used in this study are shown in Figure 2.2. The LIN model does not produce a linear curve because the presence of nonlinear geometry is accounted for at large deformations. The same material properties were used for the tibial and femoral cartilages. The LIN, NH, and PE material models used for this study were existing material models in the Abaqus material library.

Table 2.2: Material properties and references for LIN, NH, and PE cartilage material models. E = Young's Modulus, v = Poisson's ratio, μ = Shear Modulus, K = Bulk Modulus, e_0 = initial void ratio, k = permeability.

Material Model	Material Properties	Source
LIN	E = 15 MPa, v = 0.475	[13]
NH	μ = 5.084 MPa, K = 100 Mpa	[13]
PE	E = 10 MPa, v = 0.15, e_0 = 4, k = 1 * 10^{-15} m^4/N s	[34]

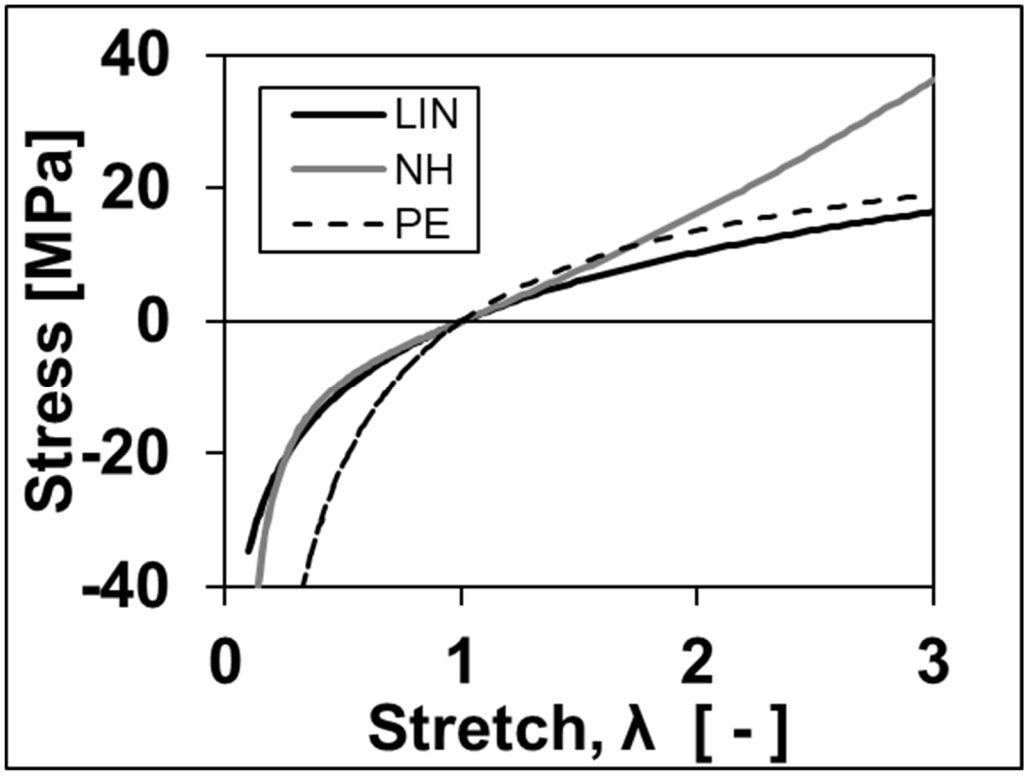

Figure 2.3: FE predictions of stress for a single element in uniaxial loading using LIN, NH, and PE material models with material properties given in Table 2.2.

Menisci were modeled as a transversely isotropic, linear elastic material with E_1 = 120 MPa, $E_{2,3}$ = 20 MPa, $G_{12,13}$ = 57.7 MPa, G_{23} = 8.33 MPa, $v_{12,13}$ = 0.3, v_{23} = 0.2 [10] where the 1 direction was the circumferential direction, 2 was the radial direction, 3 was the axial direction, G was a shear modulus, and v was the Poisson's ratio. In this study the ligaments included distinct bundles of the anterior cruciate ligament (ACL), posterior cruciate ligament (PCL), medial collateral ligament (MCL), and lateral collateral ligament (LCL). Ligament and meniscal attachments were modeled using 1-D nonlinear springs [12, 14, 15, 38, 39, 41, 46, 54, 56, 68]. Meniscal attachments connected the anterior and posterior ends of the meniscus to the nearby surface of the tibia. There were 10 spring elements modeling the ligaments and 64 spring elements modeling the

meniscal attachments. In Abaqus the springs were implemented as “SpringA” elements defined by a force-displacement data series capable of modeling nonlinearity and pretension in ligaments. Ligament stiffness and slack lengths are given for each ligament spring element in Table 2.3 and meniscal attachments had a combined stiffness of 2000N/mm [46, 48]. Bones were modeled as rigid bodies [56].

Table 2.3: Ligament stiffness and slack both normalized by length [46].

Ligament Bundle	Insertion Site	Stiffness [N / -]	Slack Length [-]
ACL	Anterior	5000	0.94
ACL	Posterior	5000	0.9
PCL	Anterior	9000	1.24
PCL	Posterior	9000	1.03
MCL	Anterior	2750	0.96
MCL	Posterior	2750	0.97
MCL	Inferior	2750	0.96
LCL	Anterior	2000	1.25
LCL	Posterior	2000	0.92
LCL	Superior	2000	1.05

Boundary Conditions and Constraints

Contact was modeled between femoral and tibial cartilages, femoral cartilage and menisci, and tibial cartilage and menisci using surface-to-surface contact pair definitions and hard contact enforcement settings. The interactions between all bodies were assumed to be frictionless. Loading cases selected to match experimental loading [47] shown in Table 2.4 were applied to each model (Figure 2.4) using LIN, NH, and PE cartilage material models. The boundary

conditions (Figure 2.4) for each loading case were specified to match an experimental procedure where anterior-posterior translation, medial-lateral translation, and internal-external rotation were free and the remaining degrees of freedom were constrained [47].

Table 2.4: Applied joint compression forces and flexion angles.

Loading Cases	Compression Force [N]	Knee Flexion [degree]
1	500	0
2	1000	0
3	1000	30

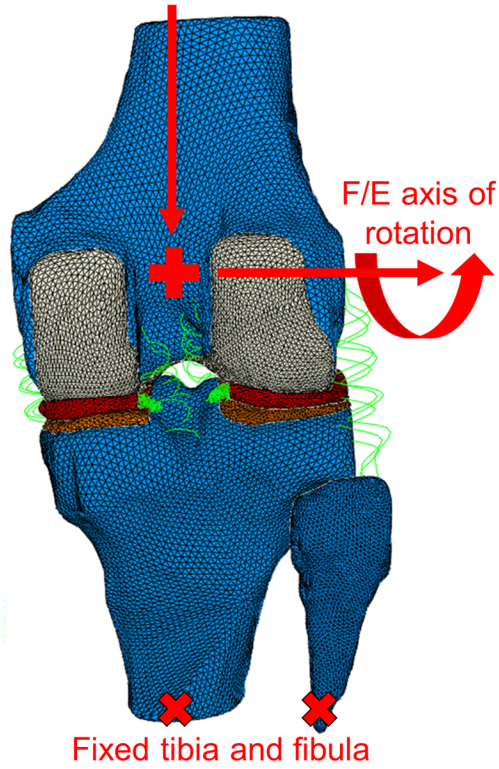

Figure 2.4: Compression force load was applied to the femur at the plus sign marker and knee flexion angle was applied to the femur about the axis shown. Tibia and fibula were fixed in the compression force direction.

Statistical Analysis

One-way ANOVA and post-hoc Tukey tests were performed for FE predictions of cartilage contact pressure using LIN, NH, and PE cartilage materials models averaged for all subjects at each loading case. The experimental study [47] was performed using 10 cadavers (6 male, 4 female, age = 44.5 ± 15.5) and had no common subjects with this study. A confidence interval of 95% was used to determine significant statistical differences at each loading case. In addition, mean results using LIN, NH, and PE material models at each loading case were compared to mean experimental results [47] using t-tests ($p < 0.05$ significant). A posteriori power analyses were performed to determine the number of knee models needed to determine significant statistical differences at each loading case.

CHAPTER 3

RESULTS

LIN, NH, and PE cartilage contact pressure predictions averaged for all subjects are given in Table 3.1 and Figure 3.1. Contour plot results for all model simulations are provided in Appendix C. One-way ANOVA showed no significant statistical differences between LIN, NH, and PE cartilage contact pressure predictions considered separately at each load and separately for medial (M) and lateral (L) tibial cartilage compartments (500N: M $p=0.14$, L $p=0.73$; 1000N: M $p=0.40$, L $p=0.75$; 1000N at 30 degrees: M $p=0.20$, L $p=0.57$). One-way ANOVA and post-hoc Tukey test results comparing LIN, NH, and PE predictions in each compartment for all loading cases are given in Appendix D. Although there were no statistical differences for the 500N load in the medial compartment, the p-value of 0.14 indicated that it may be close to significance and a power analysis at a power of 80% suggested 4 knee models would be needed for the analysis to show significant differences in cartilage contact pressures predicted by LIN, NH and PE material models. For the 1000N load applied to 30 degrees in the medial compartment, the p-value of 0.20 also did not show significance, but, again, a power analysis indicated 8 knee models would be needed to show significance in the material model comparisons. PE predicted standard deviations were greater than LIN and NH prediction standard deviations for all loading cases. LIN, NH, and PE predictions had greater standard deviations in the lateral compartment compared to the medial compartment for all loading cases.

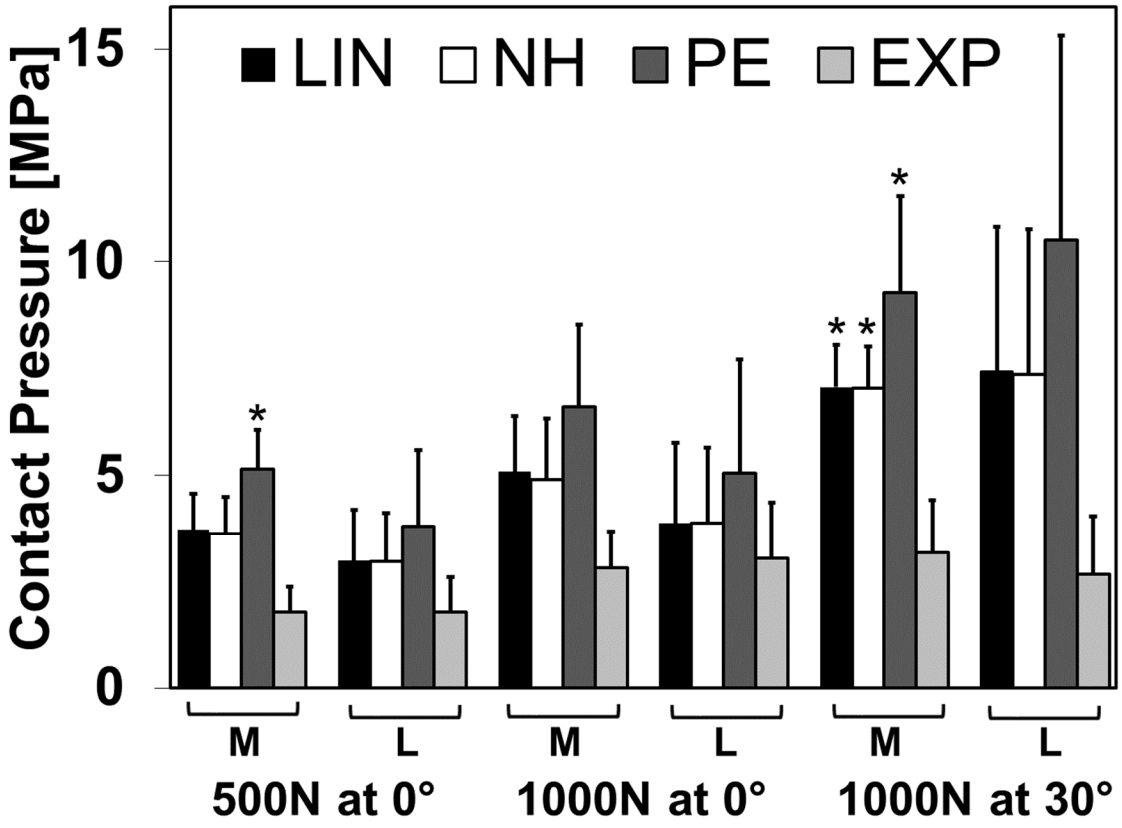

Figure 3.1: LIN, NH, and PE tibial cartilage contact pressure mean and standard deviations for all loading cases. EXP = experimental results are from a cadaver study [47]. * = significantly different from experimental results.

Table 3.1: LIN, NH, and PE tibial cartilage contact pressure mean and standard deviations for all loading cases. EXP = experimental results are from a cadaver study [47]. * = significantly different from experimental results.

	500N at 0°		1000N at 0°		1000N at 30°	
	M	L	M	L	M	L
	[MPa]	[MPa]	[MPa]	[MPa]	[MPa]	[MPa]
LIN	3.72 ± 0.86	2.99 ± 1.21	5.09 ± 1.31	3.88 ± 1.88	7.07 ± 1.00*	7.42 ± 3.42
NH	3.64 ± 0.87	2.97 ± 1.15	4.90 ± 1.43	3.88 ± 1.76	7.05 ± 0.97*	7.37 ± 3.42
PE	5.15 ± 0.92*	3.80 ± 1.80	6.61 ± 1.93	5.06 ± 2.65	9.29 ± 2.28*	10.50 ± 4.83
EXP	1.78 ± 0.60	1.79 ± 0.82	2.82 ± 0.87	3.04 ± 1.32	3.19 ± 1.23	2.68 ± 1.36

Medial cartilage contact pressure predictions for the 1000N compressive force at 30 degrees were greater than 1000N compressive force at zero degrees

for all three material models for subjects 1 and 3 (Appendix A). PE cartilage material model predictions for the 1000N compressive force at 30 degrees had the largest discrepancy between medial and lateral loading with no clear trend amongst subjects 1, 2, and 3. For the 1000N compressive force at 30 degrees using the PE material model, subject 1 predicted 185% greater pressure in the medial compared to the lateral, subject 2 predicted 210% greater pressure in the lateral compared to the medial, and subject 3 predicted 110% greater pressure in the lateral compared to the medial compartment. Medial cartilage pressure was greater than the lateral cartilage pressure for every material model for every subject at 0 degrees for both 500N and 1000N (Appendix A).

At 500N the mean LIN and NH predictions were within two standard deviations of the experimental results for the lateral compartment and exceeded three standard deviations of the experimental results for the medial compartment. Both the LIN and the NH material models predicted cartilage pressures statistically similar to the experimental results at the 500N load for both the medial and lateral compartments. At 500N the mean PE predictions were within three standard deviations of the experimental results for the lateral compartment and exceeded three standard deviations of the experimental results for the medial compartment, with the statistical analysis indicating the PE material model overpredicted the experimental results for the medial compartment ($p=0.027$, Figure 3.1, Table 3.1). At 1000N applied at 0 degrees the mean values of LIN and NH predictions were within three standard deviations of the experimental results for the medial compartment and within one standard deviation of

experimental results for the lateral compartment. No statistical differences were found between either the LIN or NH material model predictions compared to the experimental results at the 1000N load applied at 0 degrees. At 1000N applied at 0 degrees the mean values of the PE predictions were within two standard deviations of the experimental results for the lateral compartment and exceeded three standard deviations of the experimental results for the medial compartment, but the statistical analysis found similarities between the PE predictions and the experimental results for both compartments. At 1000N applied at 30 degrees the mean values of LIN, NH, and PE exceeded three standard deviations of the experimental results for both medial and lateral compartments. The statistical analysis found statistical differences between the LIN ($p=0.0050$), NH ($p=0.0048$), and PE ($p=0.047$) material models compared to the experimental results for the medial compartment at the 1000N load applied at 30 degrees (Figure 3.1, Table 3.1). No statistical differences were found for the lateral compartment.

CHAPTER 4

DISCUSSION

This study is the first to report FE cartilage contact pressure predictions for LIN, NH, and PE material models for three subjects at multiple load cases. The goal to investigate LIN, NH, and PE predictions of cartilage contact pressure using subject-specific models was sufficiently met. FE and experimental measurements of cartilage contact pressure only showed significant statistical differences for LIN, NH, and PE predictions in the medial compartment at 1000N applied at 30 degrees, and for the PE prediction in the medial compartment at 500N applied at 0 degrees. The hypothesis of this study asserted that FE predictions of cartilage contact pressure using the PE cartilage material model would be more similar to experimental data than the LIN and NH cartilage material models and this was determined to be incorrect. FE predictions of cartilage contact pressure using the PE cartilage material model were considered less similar to experimental data than LIN and NH cartilage material models because in the medial compartment they were statistically different for two loading cases compared to the LIN and NH which were statically different for one loading case.

Past studies comparing FE predictions using a LIN cartilage material model with experimental in-vivo MRI measurements found close agreement in contact area and contact deformation [48]. A past study also compared FE predictions and experimental cadaver measurements of cartilage contact pressure and reported finding strong correlation in the A-P position of the center

of pressure [49]. A published study compared FE model predictions with separately published experimental results and found good agreement between contact area and femoral displacement for three load cases using one subject [50]. The current study does not directly refute any of the findings of these past studies comparing FE predictions with experiments, but contributes to their findings by reporting for which loads significant statistical differences between FE cartilage contact predictions using LIN, NH, PE cartilage material models and experiments exists.

A published study compared FE model predictions for LIN, PE, Transversely-Isotropic, and Fibril-Reinforced Poroelastic cartilage material models and clearly demonstrated that LIN and PE material models could not simultaneously capture maximum principal stress in the cartilage [34]. A study comparing FE predictions using Linear-isotropic (LIN) and transversely-isotropic material property modulus values found positive correlations between increasing moduli and cartilage contact pressure [40]. A study compared depth-dependent fibril-reinforced cartilage models with LIN material models and found that LIN predictions of cartilage contact pressure were 19% and 30% less for mean and peak pressure, respectively [41]. A study predicted cartilage contact pressure in the tibiofemoral and patellofemoral joints with LIN material cartilage model having a varying Poisson's ratio found changes in contact pressure [51]. The current study does not directly refute any of the findings of these past studies comparing FE predictions using different material models, but contributes to the findings by

reporting cartilage contact predictions for three subjects using LIN, NH, and PE cartilage materials models for three loading cases.

One limitation in this study is the properties selected for each material model. Articular cartilage may exhibit mechanical characteristics of a heterogeneous, fibril-reinforced, depth-dependent, time dependent, multi-phasic material depending on the loading case [52]. The LIN, NH, and PE material models implemented in this study are homogenous elastic isotropic material models. The material properties for each cartilage material model used in this study were taken from references where cartilage explants from cadavers were measured and subsequently utilized in several published knee model studies for LIN and NH [10, 18, 48, 49], and PE [34]. Amongst published studies using LIN models there are examples of knee cartilage moduli of 5 MPa [21, 53, 54], 10 MPa [51, 55], 15 MPa [13, 14, 56–58], 20 MPa [34], and 25 MPa [10]. LIN, NH, and PE cartilage material models in this study were assigned the same material property parameters for each subject. Selected material properties used for this study do not account for the possibility of subject variability. Although each subject is male and approximately the same age there is still the possibility of variation in material properties that is entirely unaccounted for in this study.

Another limitation of this study is how the geometries of each model were defined. It was challenging to create accurate subject-specific geometries with sufficient tetrahedral quality due to developmental time constraints, user-identification error, and inconsistencies in surface processing and mesh generation. Femoral and tibial cartilage boundaries in the knee were challenging

to clearly delineate at both the bone-cartilage and cartilage-cartilage interfaces. An automated segmentation process to delineate the cartilage, menisci, and bone boundaries in a quantitative manner could be expected to produce more consistent knee model geometry but is sufficiently complicated to necessitate an entire study to develop and validate the models. As such it was necessary in this study to constantly make visual assessments of the cartilage boundaries and an uncertainty in cartilage layer thickness may have affected cartilage contact pressure predictions. The menisci boundary in contact with the cartilage was very visibly defined but the menisci boundary with the greater knee joint capsule was much less clearly defined. The three-dimensional surfaces of the menisci were continually evaluated during their segmentation process in order to ensure they did not include excessive tissues to the best of the modeler's visual assessment.

The present study was limited in having only three subjects and as such suffered from being less likely to find statistically significant differences in FE predictions using LIN, NH, and PE cartilage material models. Power analysis at a power of 80% suggested 4 knee models would be needed for the statistical analysis to show significant difference in cartilage contact pressures predicted in the medial compartment using LIN, NH, and PE material models at 500N load applied at 0 degrees. Power analysis at a power of 80% also suggested that 8 knee models would be needed to show significant differences in cartilage contact pressure predicted in the medial compartment using LIN, NH, and PE material models at 1000N load applied at 30 degrees. It is reasonable to assume that

statistical significance would have been found between the material models in these FE predictions if more knee models were included in the analyses. In addition it is worth noting that significant statistical differences were only found in the medial compartment. Medial and lateral compartment load sharing is known to be affected by knee coordinate axis selection, especially at high angles, and a more reliable method for determining an accurate knee coordinate axis system would benefit future studies, especially studies where large rotations, loads, and moments about several axes are applied. A future study increasing the number of subjects from 3 to 4 or 8 subjects would be a feasible goal given the methodology of this current study. A future study that included 8 subjects could be expected to require 200-300 of hours of additional time in model development alone and it was not feasible to increase the number of subjects from 3 in the current study.

In future studies the accuracy of in-vivo cartilage contact pressure predictions could possibly be improved by determining subject-specific cartilage material properties using Quantative MRI (QMRI) [59–62] or in-vivo loading during MRI with displacement-encoded imaging [63, 64]. Both QMRI and in-vivo loading during MRI with displacement-encoded imaging are sufficiently complicated to warrant an entire study and require extensive analysis and specialized experimental protocols. Published material property results for femoral and tibial cartilage using in-vivo loading during MRI and digital image correlation have reported large standard deviations and as such would potentially motivate studies where a range of cartilage contact pressures are reported.

The differences between the FE predictions and the experimental results [47] were the cause of several limitations in this study. The participants for the FE study were not the same participants for the experimental study. Participants for the FE study had an age of 22±1 years and the experimental study cadavers had an age of 44.5±15.5 years. In addition, the participants of the FE study were entirely male and the experiment study cadavers were 6 male and 4 female. There was no information given on experimental study cadaver BMI so it was not possible to compare with the BMI of the participants of the FE study. Differences in age, gender, and BMI between participants of the FE study and the experiment are undesirable and may have resulted in different cartilage properties and thicknesses between the FE models and the experimental participants, which may have affected the cartilage pressure results between the two groups.

In conclusion this study developed methods for accurately creating multiple subject-specific tibiofemoral knee joint FE models from MRI. This study compared FE predictions of cartilage contact pressure for multiple subjects and reported significant statistical differences of each material model with experimental results in the medial compartment using the LIN, NH, and PE cartilage material models for the 1000N load applied at 30 degrees and in the medial compartment using the PE cartilage material model for the 500N load applied at 0 degrees. The hypothesis that FE predictions of cartilage contact pressure using the LIN and NH cartilage material models would have more significant statistical differences to experimental results than the PE cartilage material models at all loads was found to be incorrect. FE predictions of cartilage

contact pressure using the LIN and NH cartilage material models were not statistically different to the experimental results in the lateral compartment for all three loading cases and in the medial compartment for 500N and 1000N loading cases applied at 0 degrees. The results of this study demonstrated that future subject specific knee joint FE studies would be justified in selecting either LIN or NH cartilage material models for the purpose of making FE predictions of cartilage contact pressure. Past studies that have made FE predictions using the LIN cartilage material model reported good agreement with experimental results for cartilage deformation, contact area, and contact center of pressure location [48, 49]. Overall the LIN cartilage material model has been the most widely used in past studies and it the most obvious choice for an isotropic, homogenous cartilage material model due to the availability of material properties reported in past studies. It is recommended that future subject specific models use the LIN material model because of its ease to implement in tibiofemoral joint FE models.

REFERENCES

[1] A. D. Woolf and B. Pfleger, “Burden of major musculoskeletal conditions,” *Bull. World Health Organ.*, vol. 81, no. 9, pp. 646–656, 2003.

[2] C. J. L. Murray and A. D. Lopez, “Burden of Disease: A comprehensive assessment of mortality and disability from diseases, injuries, and risk factors in 1990 and projected to 2020,” Geneva, Switzerland, 1996.

[3] M. Cross *et al.*, “The global burden of hip and knee osteoarthritis: estimates from the Global Burden of Disease 2010 study,” *Ann. Rheum. Dis.*, vol. 73, no. 7, pp. 1323–1330, 2014.

[4] R. C. Lawrence *et al.*, “Estimates of the Prevalence of Arthritis and Other Rheumatic Conditions in the United States Part II,” *ARTHRITIS Rheum.*, vol. 58, no. 1, pp. 26–35, 2008.

[5] E. Losina, T. S. Thornhill, B. N. Rome, J. Wright, and J. N. Katz, “The Dramatic Increase in Total Knee Replacement Utilization Rates in the United States Cannot Be Fully Explained by Growth in Population Size and the Obesity Epidemic,” *J. bone Jt. Surg.*, vol. 94, pp. 201–207, 2012.

[6] S. Kurtz, K. Ong, E. Lau, F. Mowat, and M. Halpern, “Projections of primary and revision hip and knee arthroplasty in the United States from 2005 to 2030,” *J. Bone Jt. Surg.*, vol. 89, no. 4, pp. 780–5, 2007.

[7] E. Losina *et al.*, “Cost-effectiveness of total knee arthroplasty in the United States: Patient risk and hospital volume,” *Arch. Intern. Med.*, vol. 169, no. 12, pp. 1113-1122, 2009.

[8] C. R. Henak, A. E. Anderson, and J. A. Weiss, “Subject-Specific Analysis

of Joint Contact Mechanics: Application to the Study of Osteoarthritis and Surgical Planning." *J. Biomech. Eng.*, vol. 135, pp. 021003-26, 2013.

[9] G. A. Ateshian, C. R. Henak, and J. A. Weiss, "Toward patient-specific articular contact mechanics," *J. Biomech.*, vol. 48, no. 5, pp. 779–786, 2015.

[10] R. Mootanah *et al.*, "Development and validation of a computational model of the knee joint for the evaluation of surgical treatments for osteoarthritis.," *Comput. Methods Biomech. Biomed. Engin.*, vol. 17, no. 13, pp. 1502-1517, 2014.

[11] E. Pena, B. Calvo, M. A. Martinez, and M. Doblare, "Effect of the size and location of osteochondral defects in degenerative arthritis. A finite element simulation," *Comput. Biol. Med.*, vol. 37, pp. 376-387, 2007.

[12] R. Shirazi and A. Shirazi-Adl, "Analysis of partial meniscectomy and ACL reconstruction in knee joint biomechanics under a combined loading," *Clin. Biomech.*, vol. 24, pp. 755-761, 2009.

[13] M. Khoshgoftar, A. C. T. Vrancken, T. G. van Tienen, P. Buma, D. Janssen, and N. Verdonschot, "The sensitivity of cartilage contact pressures in the knee joint to the size and shape of an anatomically shaped meniscal implant," *J. Biomech.*, vol. 48, pp. 1427-1435, 2015.

[14] N. Yang, H. Nayeb-Hashemi, and P. K. Canavan, "The combined effect of frontal plane tibiofemoral knee angle and meniscectomy on the cartilage contact stresses and strains," *Ann. Biomed. Eng.*, vol. 37, no. 11, pp. 2360–2372, 2009.

[15] R. Shirazi and A. Shirazi-Adl, “Computational biomechanics of articular cartilage of human knee joint: Effect of osteochondral defects,” *J. Biomech.*, vol. 42, pp. 2458-2465, 2009.

[16] M. S. Venäläinen *et al.*, “Quantitative Evaluation of the Mechanical Risks Caused by Focal Cartilage Defects in the Knee,” Sci. Rep., vol. 6, pp 37538, 2016.

[17] G. Papaioannou, C. K. Demetropoulos, and Y. H. King, “Predicting the effects of knee focal articular surface injury with a patient-specific finite element model,” *Knee*, vol. 17, pp. 61-68, 2010.

[18] H. Atmaca, C. C. Kesemenli, K. Memişoğlu, A. Özkan, and Y. Celik, “Changes in the loading of tibial articular cartilage following medial meniscectomy: A finite element analysis study,” *Knee Surgery, Sport. Traumatol. Arthrosc.*, vol. 21, pp. 2667-2673, 2013.

[19] E. Pena, B. Calvo, M. A. Martinez, D. Palnca, and M. Doblare, “Why Lateral Meniscectomy Is More Dangerous Than Medial Meniscectomy. A Finite Element Study Estefania,” *J. Orthop. Res.*, pp. 1001–1010, 2006.

[20] M. Kazemi, L. P. Li, M. D. Buschmann, and P. Savard, “Partial Meniscectomy Changes Fluid Pressurization in Articular Cartilage in Human Knees,” *J. Biomech. Eng.*, vol. 134, pp. 021001-10, 2012.

[21] E. Pena, B. Calvo, M. A. Martinez, D. Palanca, and M. Doblare, “Finite element analysis of the effect of meniscal tears and meniscectomies on human knee biomechanics,” *Clin. Biomech.*, vol. 20, no. 5, pp. 498–507, 2005.

[22] Y. Dong, G. Hu, Y. Dong, Y. Hu, and Q. Xu, “The effect of meniscal tears and resultant partial meniscectomies on the knee contact stresses: a finite element analysis.,” *Comput. Methods Biomech. Biomed. Engin.*, vol. 17, no. 13, pp. 1452-1463, 2014.

[23] T. F. Besier, G. E. Gold, S. L. Delp, M. Fredericson, and G. S. Beaupre, “The influence of femoral internal and external rotation on cartilage stresses within the patellofemoral joint,” *J. Orthop. Res.*, vol. 26, pp. 1627-1635, 2008.

[24] B. Jones, C. T. Hung, and G. Ateshian, “Biphasic Analysis of Cartilage Stresses in the Patellofemoral Joint,” *J. Knee Surg.*, vol. 29, pp. 92–98, 2015.

[25] A. A. Ali *et al.*, “Validation of predicted patellofemoral mechanics in a finite element model of the healthy and cruciate-deficient knee,” *J. Biomech.*, vol. 49, pp. 302-309, 2016.

[26] S. Pal *et al.*, “Effects of quadriceps force variability on patellofemoral cartilage stresses”, 2012.

[27] S. Pal, T. F. Besier, G. E. Gold, M. Fredericson, S. L. Delp, and G. Beaupre, “Variability in Predicted Joint Mechanics among Maltracking Patellofemoral Pain Subjects in Response to Vastus Medialis Strengthening : Implications for Rehabilitation Choices,” *Orthop. Res. Soc. Annu. Meet.*, p. 1, 2011.

[28] T. F. Besier, G. E. Gold, G. S. Beaupre, and S. L. Delp, “A modeling framework to estimate patellofemoral joint cartilage stress in vivo,” *Med.*

Sci. Sports Exerc., vol. 37, no. 11, pp. 1924–1930, 2005.

[29] T. F. Besier *et al.*, “The role of cartilage stress in patellofemoral pain,” *Med. Sci. Sports Exerc.*, pp. 2416-2422, 2015.

[30] S. Pal *et al.*, “Patellar maltracking correlates with vastus medialis activation delay in patellofemoral pain patients.,” *Am. J. Sports Med.*, vol. 39, no. 3, pp. 590–598, 2011.

[31] J. P. Halloran, S. K. Easley, A. J. Petrella, and P. J. Rullkoetter, “Comparison of deformable and elastic foundation finite element simulations for predicting knee replacement mechanics.,” *J. Biomech. Eng.*, vol. 127, no. 5, pp. 813–818, 2005.

[32] J. P. Halloran, A. J. Petrella, and P. J. Rullkoetter, “Explicit finite element modeling of total knee replacement mechanics,” *J. Biomech.*, vol. 38, no. 2, pp. 323–331, 2005.

[33] N. Czapla, “Development and Validation of a Tibiofemoral Joint Finite Element Model and Subsequent Gait Analysis of Intact ACL and ACL Deficient Individuals,” California Polytechnic State University, San Luis Obispo, 2015.

[34] O. Klets, M. E. Mononen, P. Tanska, M. T. Nieminen, R. K. Korhonen, and S. Saarakkala, “Comparison of different material models of articular cartilage in 3D computational modeling of the knee: Data from the Osteoarthritis Initiative (OAI),” *J. Biomech.*, vol. 49, pp. 3891-3900, 2016.

[35] M. E. Mononen *et al.*, “Effect of superficial collagen patterns and fibrillation of femoral articular cartilage on knee joint mechanics-A 3D finite element

analysis," *J. Biomech.*, vol. 45, pp. 579-587, 2012.

[36] V. B. Shim, T. F. Besier, D. G. Lloyd, K. Mithraratne, and J. F. Fernandez, "The influence and biomechanical role of cartilage split line pattern on tibiofemoral cartilage stress distribution during the stance phase of gait," *Biomech. Model. Mechanobiol.*, vol. 15, no.1, pp. 195-204, 2016.

[37] K. S. Halonen, M. E. Mononen, J. S. Jurvelin, J. Toyras, and R. K. Korhonen, "Importance of depth-wise distribution of collagen and proteoglycans in articular cartilage-A 3D finite element study of stresses and strains in human knee joint," *J. Biomech.*, vol. 46, pp. 1184-1192, 2013.

[38] M. G. Rumery, G. T. Lane, S. M. Klisch, and S. J. Hazelwood, "Finite Element Analysis Predictions of Knee Cartilage Contact Pressure in Gait and Dependence on Material Model Choice," in *World Congress of Biomechanics*, Dublin, Ireland, 2018.

[39] M. G. Rumery, G. T. Lane, S. M. Klisch, and S. J. Hazelwood, "Gait and Cycling Finite Element Predictions of Knee Cartilage Pressure for Linear and Porous Elastic Materials," in *Biomedical Engineering Society Annual Meeting*, Atlanta, Georgia, 2018.

[40] B. C. Marchi, E. M. Arruda, B. Benjamin, and C. Marchi, "A study on the role of articular cartilage soft tissue constitutive form in models of whole knee biomechanics," *Biomech. Model. Mechanobiol., vol. 16, no. 1, 2016.*

[41] M. Adouni, A. Shirazi-Adl, and R. Shirazi, "Computational biodynamics of human knee joint in gait: From muscle forces to cartilage stresses," *J.*

Biomech., vol. 45, pp. 2149-2156, 2012.

[42] J. A. Buckwalter, D. D. Anderson, T. D. Brown, Y. Tochigi, and J. A. Martin, "The Roles of Mechanical Stresses in the Pathogenesis of Osteoarthritis-Implications for Treatment of Joint Injuries," *Cartilage*, pp. 1–9, 2013.

[43] P. A. Yushkevich *et al.*, "User-guided 3D active contour segmentation of anatomical structures: Significantly improved efficiency and reliability," *Neuroimage*, vol. 31, no. 3, pp. 1116–1128, 2006.

[44] P. Cignoni, M. Callieri, M. Corsini, M. Dellepiane, F. Ganovelli, and G. Ranzuglia, "MeshLab: an Open-Source Mesh Processing Tool."

[45] H. Si, "TetGen, a Quality Tetrahedral Mesh Generator," *AMC Trans. Math. Softw.*, vol. 41, no. 2, p. 11, 2015.

[46] L. Blankevoort, J. H. Kuiper, R. Huiskes, and H. J. Grootenboer, "Articular contact in a three-dimensional model of the knee," *J. Biomech.*, vol. 24, no. 11, pp. 1019–1031, 1991.

[47] A. M. Seitz, A. Lubomierski, B. Friemert, A. Ignatius, and L. Dürselen, "Effect of partial meniscectomy at the medial posterior horn on tibiofemoral contact mechanics and meniscal hoop strains in human knees," *J. Orthop. Res.*, vol. 30, pp. 934-942, 2012.

[48] K.-T. Kang, S.-H. Kim, J. Son, Y. H. Lee, and H.-J. Chun, "In Vivo Evaluation of the Subject-Specific Finite Element Model for Knee Joint Cartilage Contact Area," *Int. J. Precis. Eng. Manuf.*, vol. 16, no. 6, pp. 1171–1177, 2015.

[49] A. Kiapour *et al.*, "Finite Element Model of the Knee for Investigation of

Injury Mechanisms: Development and Validation," *J. Biomech. Eng.*, vol. 136, pp. 011002-14, 2013.

[50] Q. Meng, Z. Jin, R. Wilcox, and J. Fisher, "Computational investigation of the time-dependent contact behaviour of the human tibiofemoral joint under body weight," *Proc. Inst. Mech. Eng. Part H J. Eng. Med.*, vol. 228, no. 11, pp. 1193–1207, 2014.

[51] Y. Wang, Y. Fan, and M. Zhang, "Comparison of stress on knee cartilage during kneeling and standing using finite element models," *Med. Eng. Phys.*, vol. 36, pp. 439-447, 2014.

[52] V. C. Mow, "Biphasic Indentation of Articular Cartilage - II. A numerical Algorithm and An Experimental Study," *J. Biomech.*, vol. 22, no. 8/9, pp. 853–861, 1989.

[53] E. Pena, B. Calvo, M. A. Martinez, and M. Doblare, "A three-dimensional finite element analysis of the combined behavior of ligaments and menisci in the healthy human knee joint," *J. Biomech.*, vol. 39, no. 9, pp. 1686–1701, 2006.

[54] G. Li, O. Lopez, and H. Rubash, "Variability of a three-dimensional finite element model constructed using magnetic resonance images of a knee for joint contact stress analysis.," *J. Biomech. Eng.*, vol. 123, no. 4, pp. 341–346, 2001.

[55] P. Łuczkiewicz, K. Daszkiewicz, W. Witkowski, J. Chróścielewski, and W. Zarzycki, "Influence of meniscus shape in the cross sectional plane on the knee contact mechanics," *J. Biomech.*, vol. 48, pp. 1356-1363, 2015.

[56] T. L. Haut Donahue *et al.*, “A Finite Element Model of the Human Knee Joint for the Study of Tibio-Femoral Contact,” *J. Biomech. Eng.*, vol. 124, no. 3, pp. 273, 2002.

[57] T. L. Haut Donahue, M. L. Hull, M. M. Rashid, and C. R. Jacobs, “How the stiffness of meniscal attachments and meniscal material properties affect tibio-femoral contact pressure computed using a validated finite element model of the human knee joint,” *J. Biomech.*, vol. 36, no. 1, pp. 19–34, 2003.

[58] Y. Dong, G. Hu, Y. Dong, Y. Hu, and Q. Xu, “The effect of meniscal tears and resultant partial meniscectomies on the knee contact stresses: A finite element analysis,” *Comput. Methods Biomech. Biomed. Engin.*, vol. 17, no. 13, pp. 1452–1463, 2014.

[59] S. J. Matzat, J. van Tiel, G. E. Gold, and E. H. G. Oei, “Quantitative MRI techniques of cartilage composition.,” *Quant. Imaging Med. Surg.*, vol. 3, no. 3, pp. 162–174, 2013.

[60] J. Schooler *et al.*, “Longitudinal evaluation of T1ρ and T2 spatial distribution in osteoarthritic and healthy medial knee cartilage,” *Osteoarthr. Cartil.*, vol. 22, no. 1, pp. 51–62, 2014.

[61] F. Eckstein, D. Burstein, and T. M. Link, “Quantitative MRI of cartilage and bone: degenerative changes in osteoarthritis,” *NMR Biomed.*, vol. 19, pp. 822–854, 2006.

[62] F. Eckstein *et al.*, “Accuracy and precision of quantitative assessment of cartilage morphology by magnetic resonance imaging at 3.0T,” *Arthritis*

Rheum., vol. 52, no. 10, pp. 3132–3136, 2005.

[63] D. D. Chan, L. Cai, K. D. Butz, S. B. Trippel, E. A. Nauman, and C. P. Neu, "In vivo articular cartilage deformation: noninvasive quantification of intratissue strain during joint contact in the human knee," *Nat. Publ. Gr.*, vol.11, no. 6, 2015.

[64] K. D. Butz, D. D. Chan, E. A. Nauman, and C. P. Neu, "Stress distributions and material properties determined in articular cartilage from MRI-based finite strains," *J. Biomech.*, vol. 44, pp. 2667-2672, 2011.

[65] P. A. Yushkevich *et al.*, "User-guided 3D active contour segmentation of anatomical structures: Significantly improved efficiency and reliability," *Neuroimage*, vol. 31, no. 3, pp. 1116–1128, 2006.

[66] P. Cignoni, M. Callieri, M. Corsini, M. Dellepiane, F. Ganovelli, and G. Ranzuglia, "MeshLab: An Open-Source Mesh Processing Tool," in *Sixth Eurographics Italian Chapter Conference*, pp. 129–136, 2008.

[67] K. M. Moerman and T. G. Badger, "Gibboncode/Gibbon: Gibbon: The Geometry And Image-Based Bioengineering Add-On (Release: Hylobates Albibarbis)," *Zenodo, Boston, MA,* 2017.

[68] G. T. Lane, "Human Knee FEA Model For Transtivial Amputee Cartilage Pressure In Gait and Cycling", California Polytechnic State University, San Luis Obispo, 2018.

Appendix A: Cartilage Contact Pressure Tables for Each Subject.

Table A.1: Tibial cartilage contact pressures for 500N load applied at 0 degree flexion angle for all subjects.

	Subject 1		Subject 2		Subject 3	
	M [MPa]	L [MPa]	M [MPa]	L [MPa]	M [MPa]	L [MPa]
LIN	3.66	2.69	4.61	4.33	2.91	1.96
NH	3.49	2.62	4.57	4.26	2.86	2.04
PE	4.41	3.56	6.18	5.71	4.86	2.13

Table A.2: Tibial cartilage contact pressures for 1000N load applied at 0 degree flexion angle for all subjects.

	Subject 1		Subject 2		Subject 3	
	M [MPa]	L [MPa]	M [MPa]	L [MPa]	M [MPa]	L [MPa]
LIN	4.09	3.42	6.57	5.95	4.59	2.26
NH	3.94	3.34	6.54	5.86	4.21	2.45
PE	4.92	4.53	8.71	7.94	6.18	2.72

Table A.3: Tibial cartilage contact pressures for 1000N load applied at 30 degree flexion angle for all subjects.

	Subject 1		Subject 2		Subject 3	
	M [MPa]	L [MPa]	M [MPa]	L [MPa]	M [MPa]	L [MPa]
LIN	8.21	5.18	6.45	11.36	6.53	5.73
NH	8.16	5.20	6.48	11.31	6.50	5.60
PE	11.87	6.40	7.56	15.82	8.42	9.30

Appendix B: Cartilage Contact Pressure Bar Graphs for Each Material Model

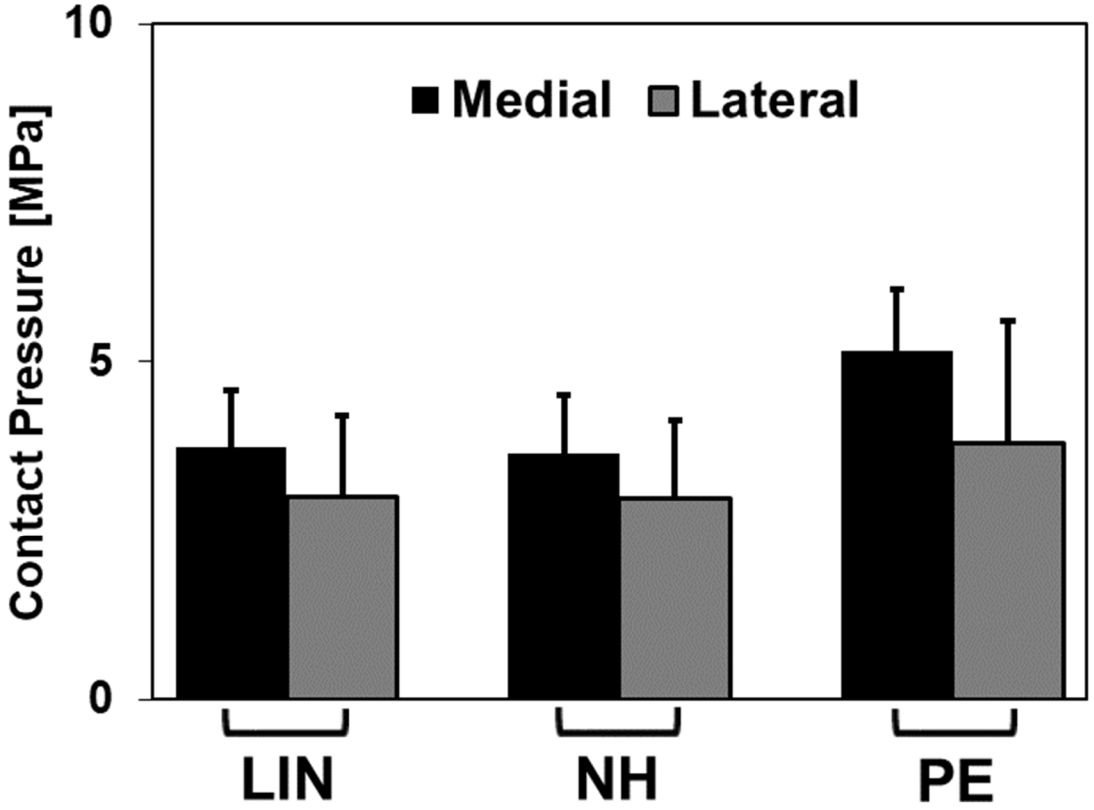

Figure B.1: Medial and lateral tibial cartilage contact pressure for 500N compression force applied at 0 degrees flexion averaged for all three subjects with error bars showing standard deviations.

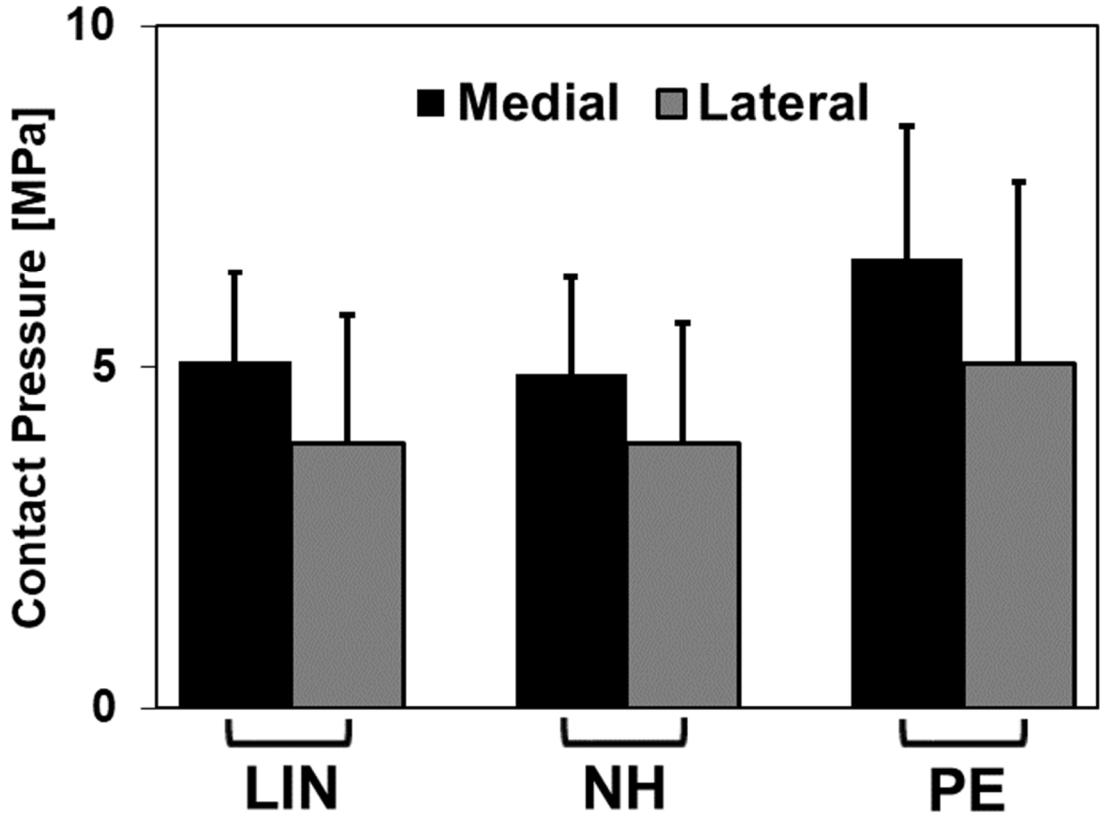

Figure B.2: Medial and lateral tibial cartilage contact pressure for 1000N compression force applied at 0 degrees flexion averaged for all three subjects with error bars showing standard deviations.

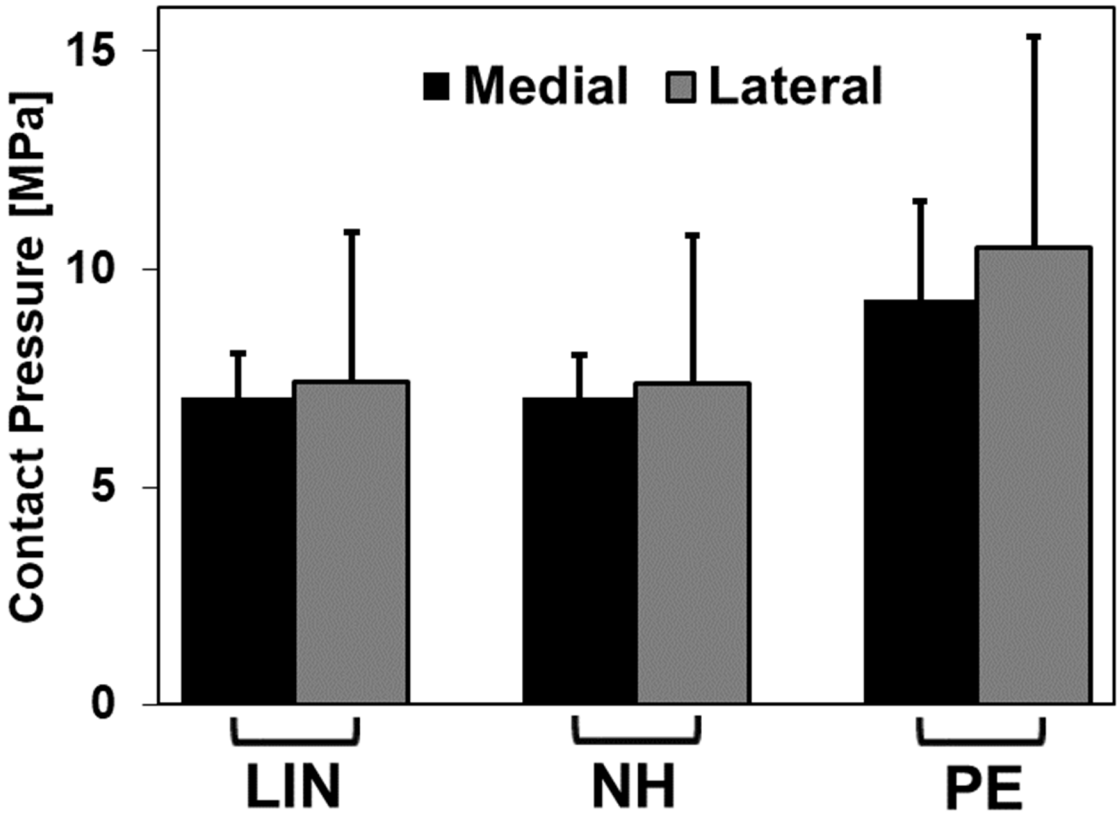

Figure B.3: Medial and lateral tibial cartilage contact pressure for 1000N compression force applied at 30 degrees flexion averaged for all three subjects with error bars showing standard deviations.

Appendix C: Cartilage Contact Pressure Contours

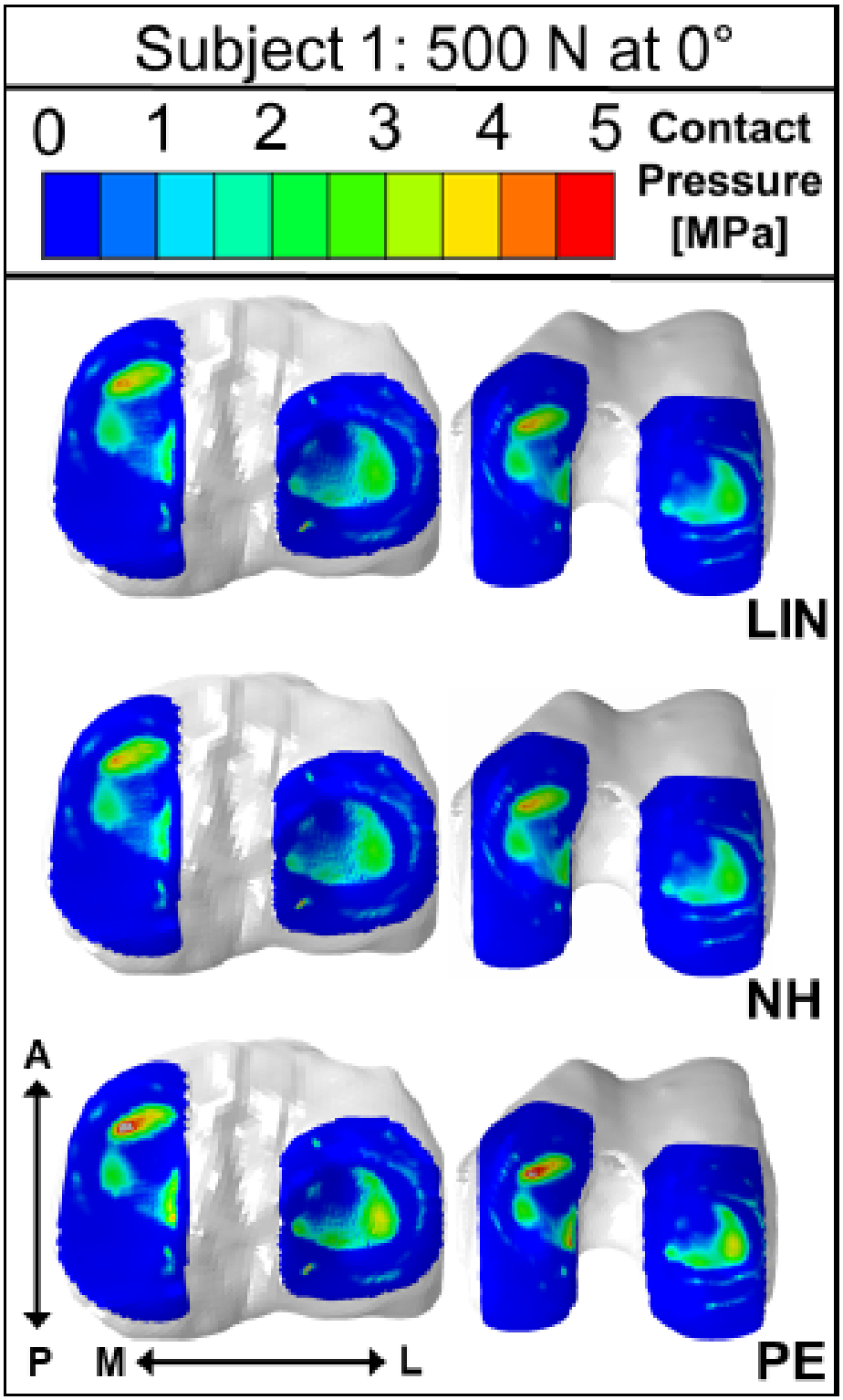

Figure C.1: Femoral and tibial cartilage contact pressure contour plots for 500N load applied at 0 degree flexion angle for subject 1.

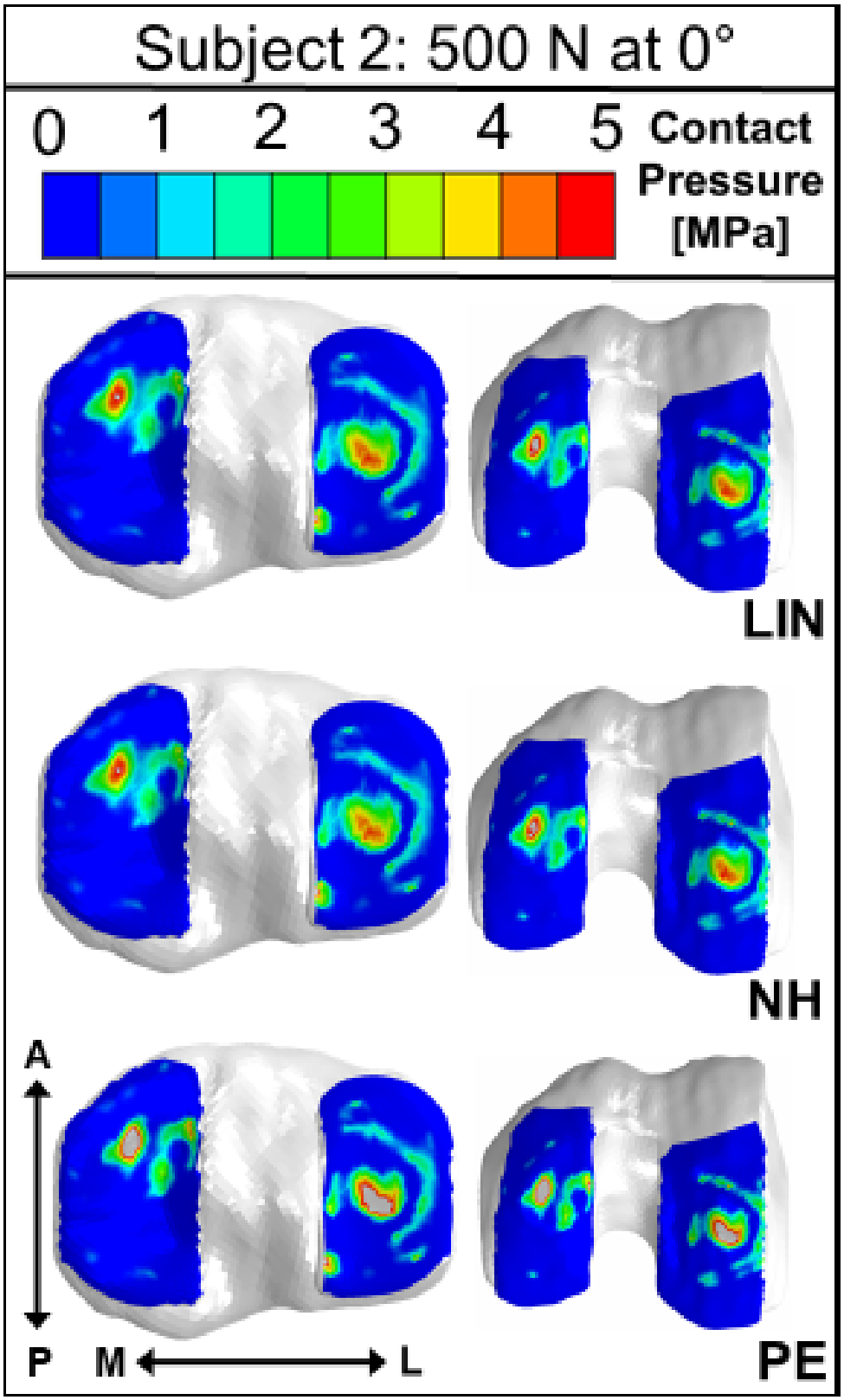

Figure C.2: Femoral and tibial cartilage contact pressure contour plots for 500N load applied at 0 degree flexion angle for subject 2.

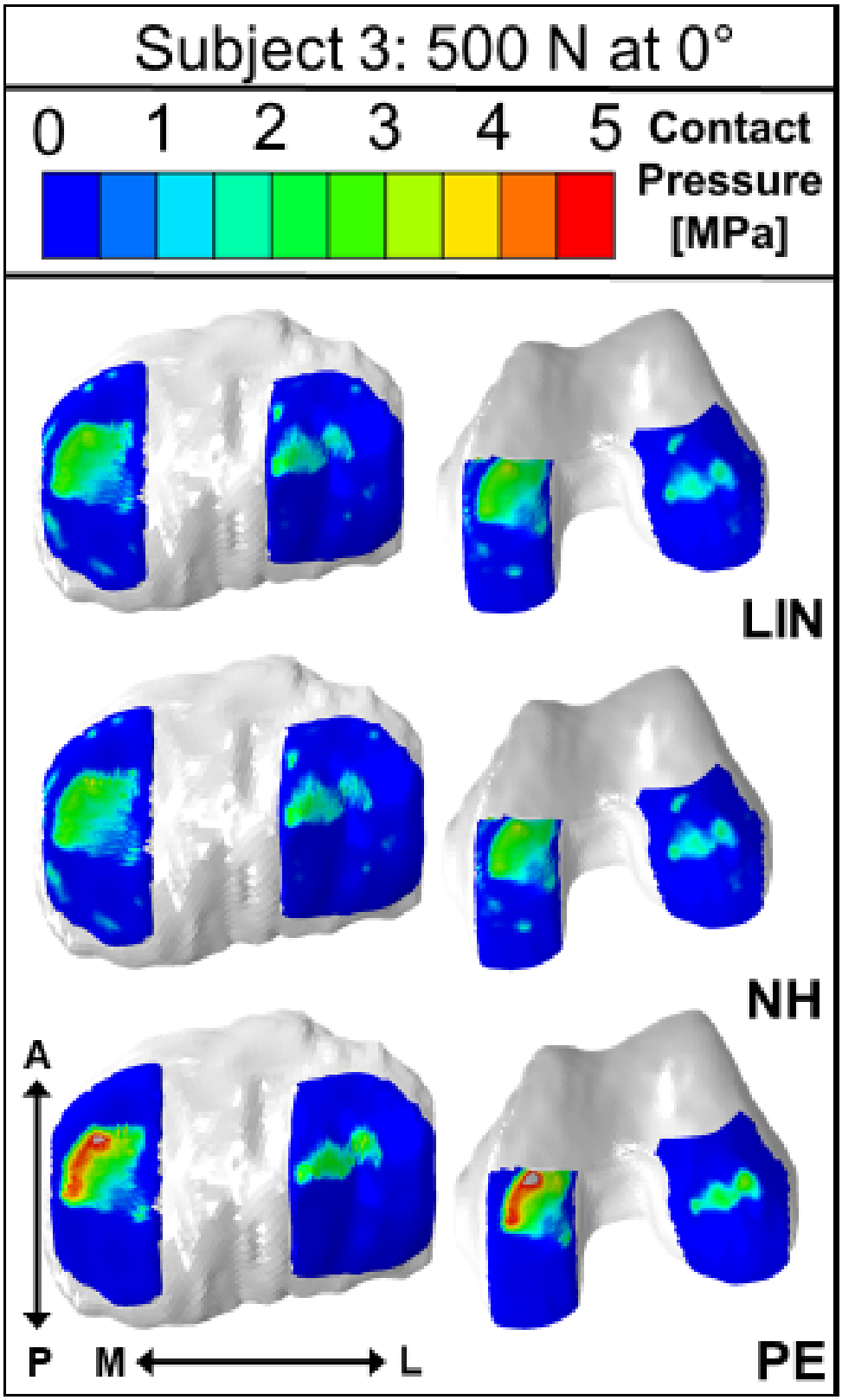

Figure C.3: Femoral and tibial cartilage contact pressure contour plots for 500N load applied at 0 degree flexion angle for subject 3.

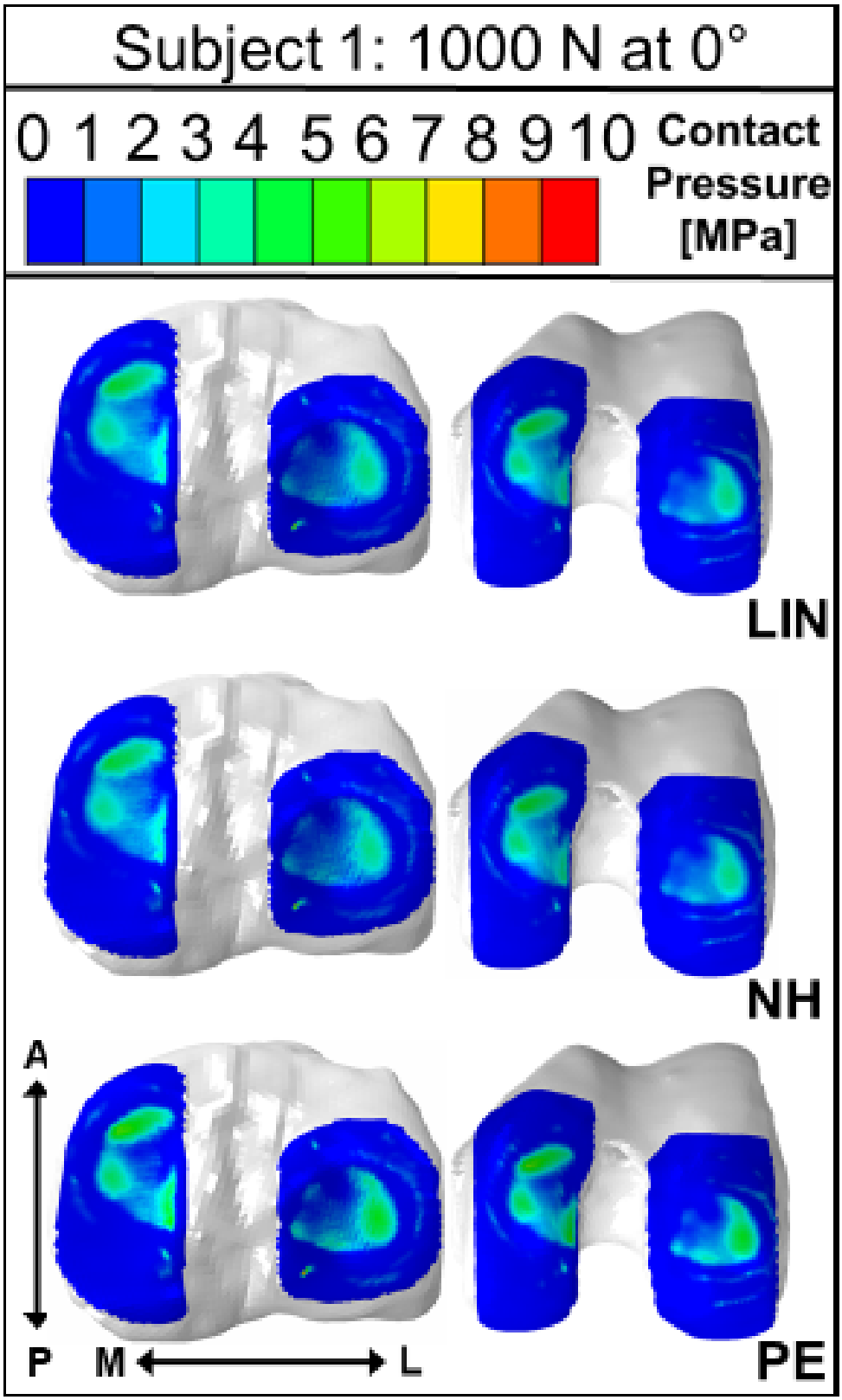

Figure C.4: Femoral and tibial cartilage contact pressure contour plots for 1000N load applied at 0 degree flexion angle for subject 1.

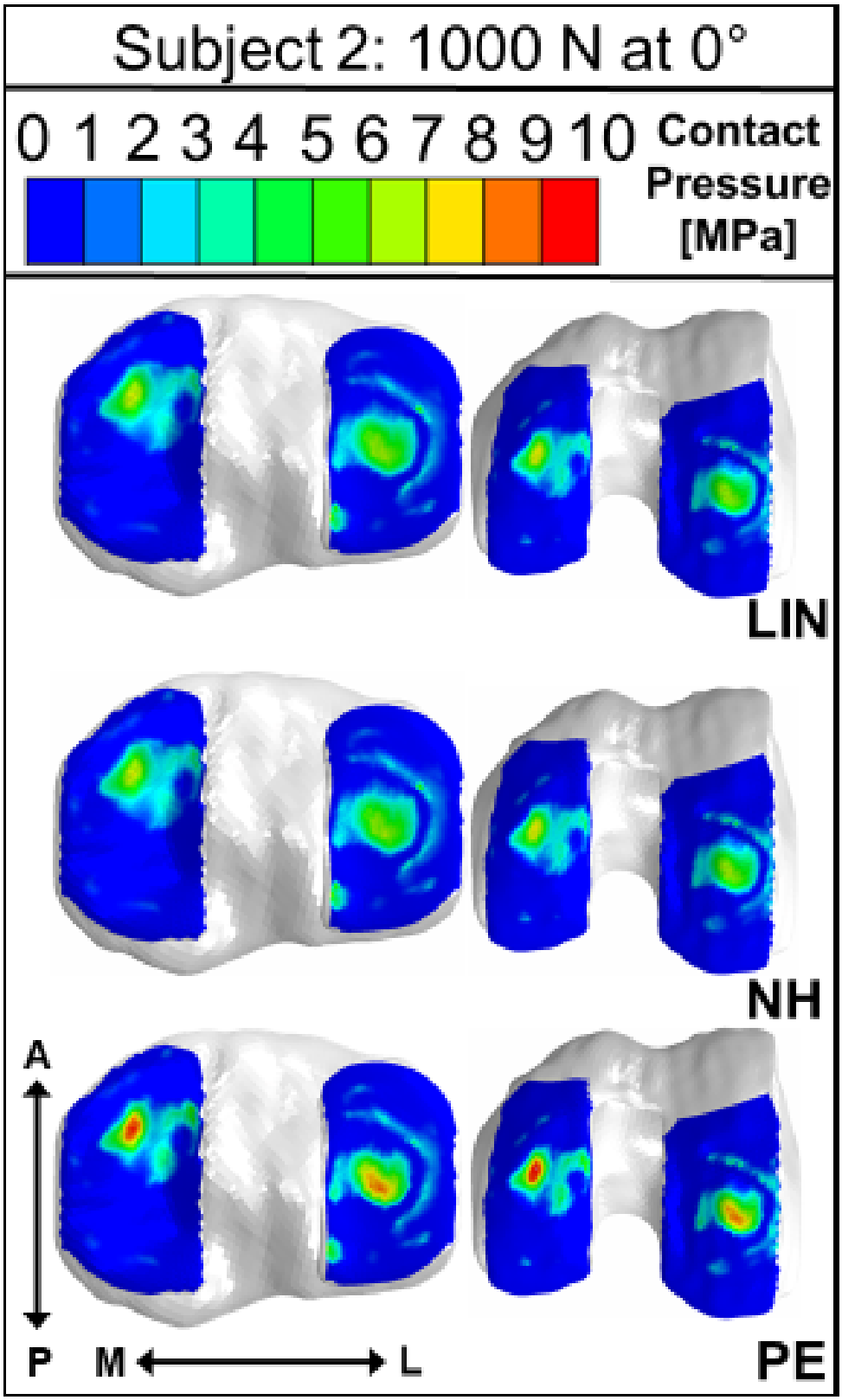

Figure C.5: Femoral and tibial cartilage contact pressure contour plots for 1000N load applied at 0 degree flexion angle for subject 2.

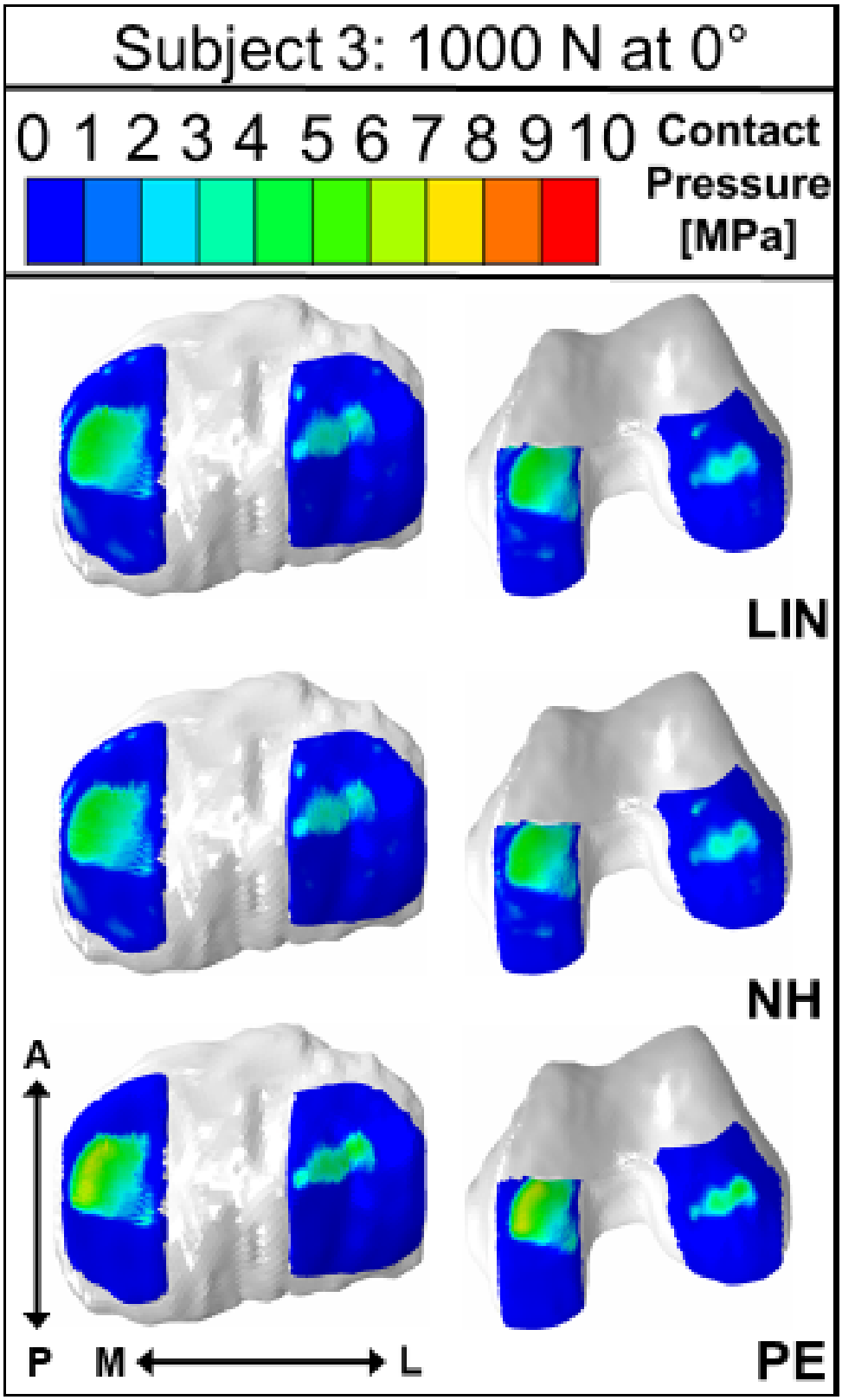

Figure C.6: Femoral and tibial cartilage contact pressure contour plots for 1000N load applied at 0 degree flexion angle for subject 3.

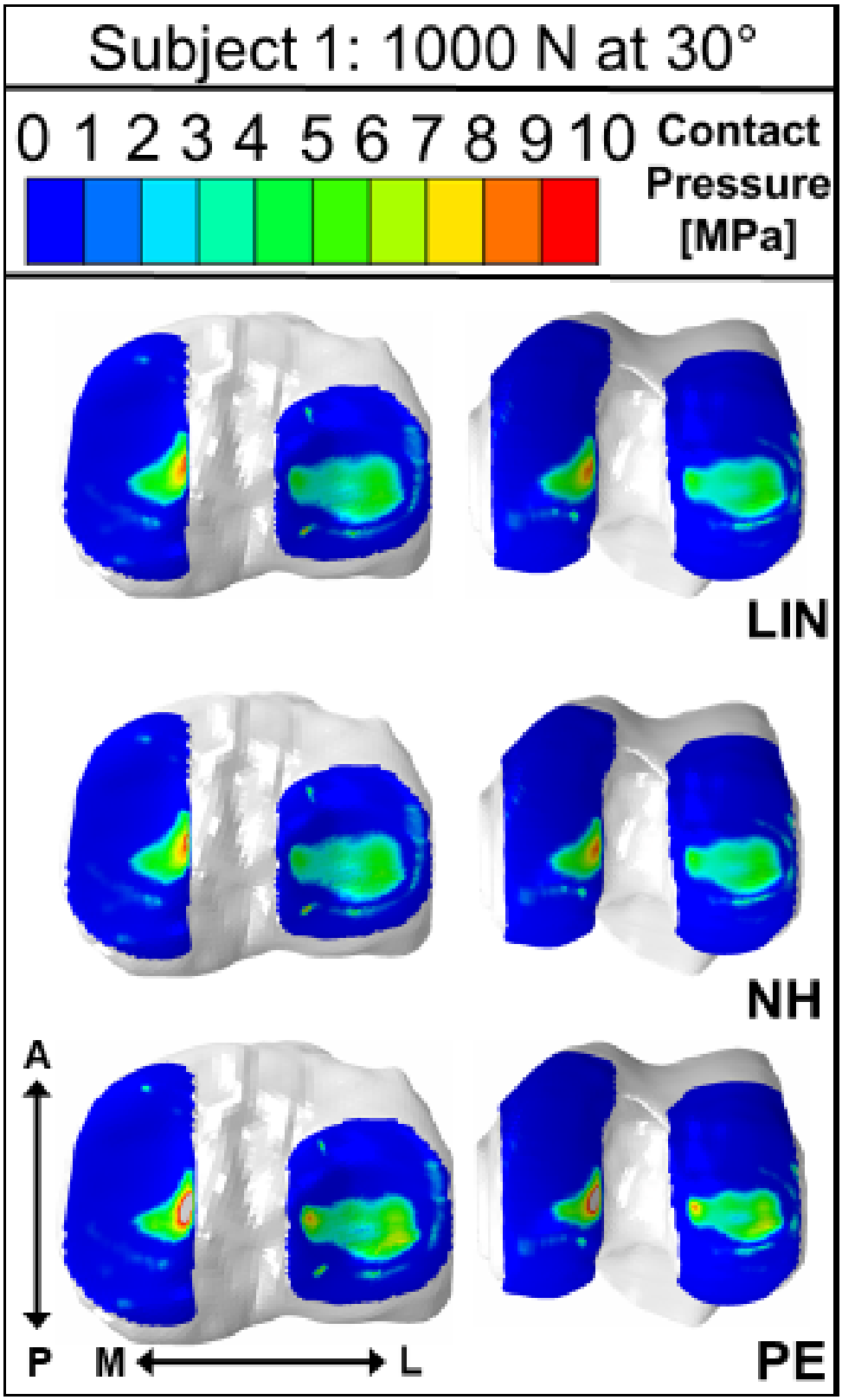

Figure C.7: Femoral and tibial cartilage contact pressure contour plots for 1000N load applied at 30 degree flexion angle for subject 1.

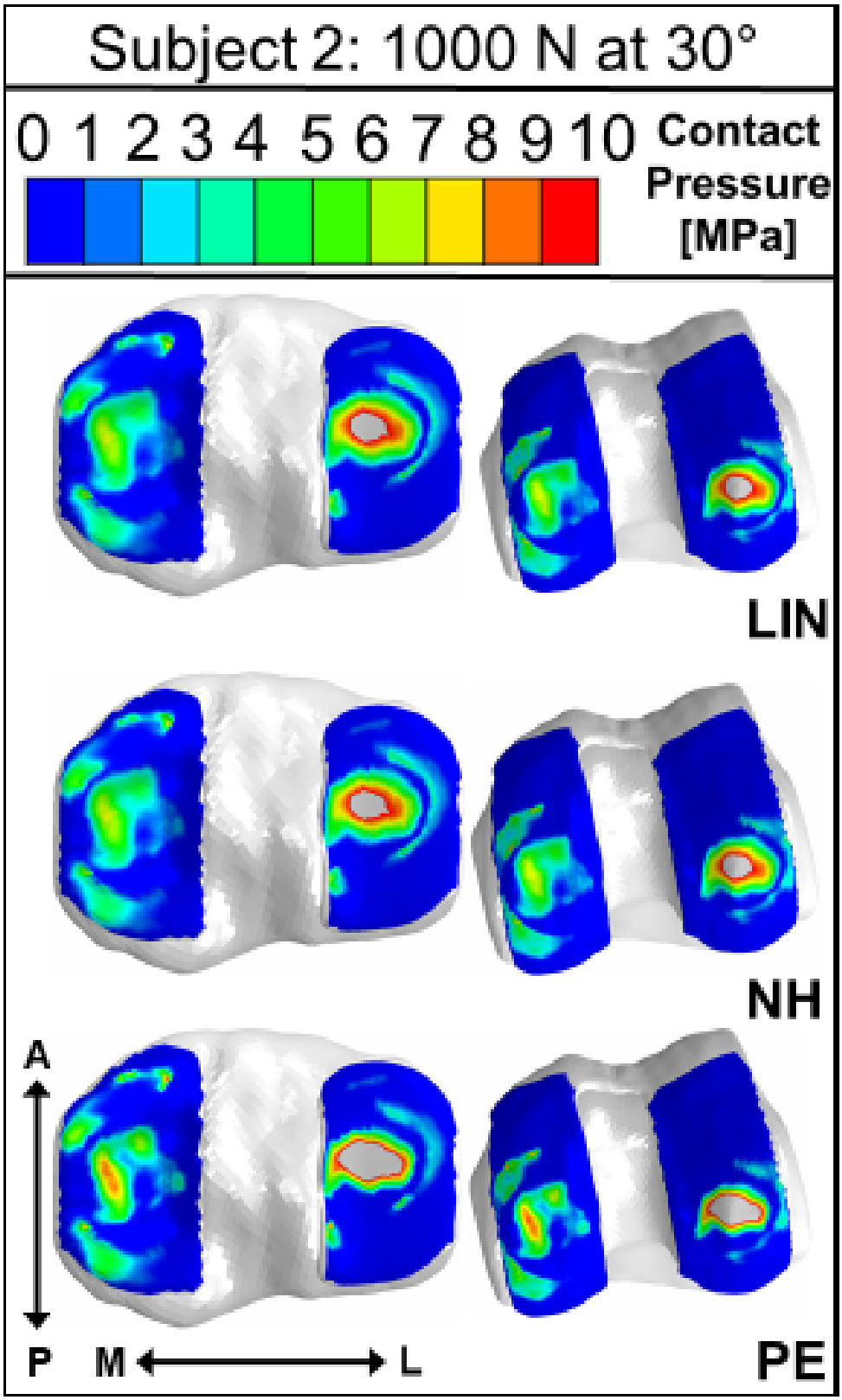

Figure C.8: Femoral and tibial cartilage contact pressure contour plots for 1000N load applied at 30 degree flexion angle for subject 2.

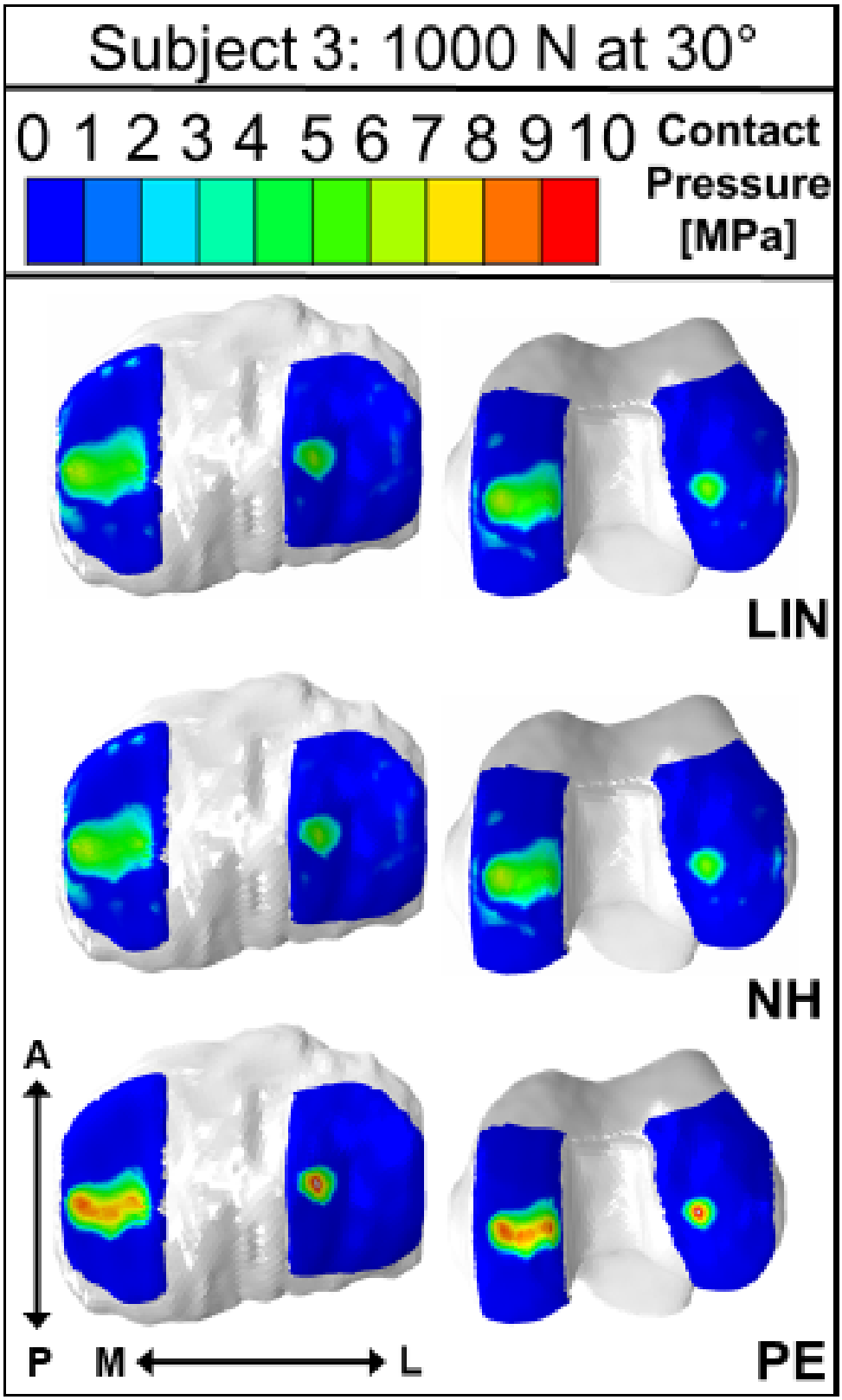

Figure C.9: Femoral and tibial cartilage contact pressure contour plots for 1000N load applied at 30 degree flexion angle for subject 2.

Appendix D: Statistical Analysis Results

One-way ANOVA: M-500-LIN, M-500-NH, M-500-PE

Method

Null hypothesis	All means are equal
Alternative hypothesis	Not all means are equal
Significance level	α = 0.05

Equal variances were assumed for the analysis.

Factor Information

Factor	Levels	Values
Factor	3	M-500-LIN, M-500-NH, M-500-PE

Analysis of Variance

Source	DF	Adj SS	Adj MS	F-Value	P-Value
Factor	2	4.317	2.1584	2.77	0.140
Error	6	4.667	0.7779		
Total	8	8.984			

Model Summary

S	R-sq	R-sq(adj)	R-sq(pred)
0.881963	48.05%	30.73%	0.00%

Means

Factor	N	Mean	StDev	95% CI
M-500-LIN	3	3.725	0.856	(2.479, 4.971)
M-500-NH	3	3.639	0.865	(2.393, 4.885)
M-500-PE	3	5.149	0.923	(3.903, 6.395)

Pooled StDev = 0.881963

Tukey Pairwise Comparisons

Grouping Information Using the Tukey Method and 95% Confidence

Factor	N	Mean	Grouping
M-500-PE	3	5.149	A
M-500-LIN	3	3.725	A
M-500-NH	3	3.639	A

Means that do not share a letter are significantly different.

Figure D.1: ANOVA and Tukey comparisons of medial tibial cartilage contact pressure for 500N load applied at 0 degree flexion angle.

One-way ANOVA: L-500-LIN, L-500-NH, L-500-PE

Method

Null hypothesis	All means are equal
Alternative hypothesis	Not all means are equal
Significance level	α = 0.05

Equal variances were assumed for the analysis.

Factor Information

Factor	Levels	Values
Factor	3	L-500-LIN, L-500-NH, L-500-PE

Analysis of Variance

Source	DF	Adj SS	Adj MS	F-Value	P-Value
Factor	2	1.336	0.6678	0.33	0.730
Error	6	12.054	2.0090		
Total	8	13.389			

Model Summary

S	R-sq	R-sq(adj)	R-sq(pred)
1.41738	9.98%	0.00%	0.00%

Means

Factor	N	Mean	StDev	95% CI
L-500-LIN	3	2.991	1.212	(0.989, 4.993)
L-500-NH	3	2.971	1.150	(0.969, 4.974)
L-500-PE	3	3.80	1.80	(1.80, 5.80)

Pooled StDev = 1.41738

Tukey Pairwise Comparisons

Grouping Information Using the Tukey Method and 95% Confidence

Factor	N	Mean	Grouping
L-500-PE	3	3.80	A
L-500-LIN	3	2.991	A
L-500-NH	3	2.971	A

Means that do not share a letter are significantly different.

Figure D.2: ANOVA and Tukey comparisons of lateral tibial cartilage contact pressure for 500N load applied at 0 degree flexion angle.

One-way ANOVA: M-1000-LIN, M-1000-NH, M-1000-PE

Method

Null hypothesis	All means are equal
Alternative hypothesis	Not all means are equal
Significance level	α = 0.05

Equal variances were assumed for the analysis.

Factor Information

Factor	Levels	Values
Factor	3	M-1000-LIN, M-1000-NH, M-1000-PE

Analysis of Variance

Source	DF	Adj SS	Adj MS	F-Value	P-Value
Factor	2	5.279	2.639	1.06	0.404
Error	6	14.983	2.497		
Total	8	20.261			

Model Summary

S	R-sq	R-sq(adj)	R-sq(pred)
1.58023	26.05%	1.40%	0.00%

Means

Factor	N	Mean	StDev	95% CI
M-1000-LIN	3	5.085	1.309	(2.853, 7.318)
M-1000-NH	3	4.896	1.433	(2.663, 7.128)
M-1000-PE	3	6.61	1.93	(4.37, 8.84)

Pooled StDev = 1.58023

Tukey Pairwise Comparisons

Grouping Information Using the Tukey Method and 95% Confidence

Factor	N	Mean	Grouping
M-1000-PE	3	6.61	A
M-1000-LIN	3	5.085	A
M-1000-NH	3	4.896	A

Means that do not share a letter are significantly different.

Figure D.3: ANOVA and Tukey comparisons of medial tibial cartilage contact pressure for 1000N load applied at 0 degree flexion angle.

One-way ANOVA: L-1000-LIN, L-1000-NH, L-1000-PE

Method

Null hypothesis	All means are equal
Alternative hypothesis	Not all means are equal
Significance level	α = 0.05

Equal variances were assumed for the analysis.

Factor Information

Factor	Levels	Values
Factor	3	L-1000-LIN, L-1000-NH, L-1000-PE

Analysis of Variance

Source	DF	Adj SS	Adj MS	F-Value	P-Value
Factor	2	2.790	1.395	0.31	0.748
Error	6	27.409	4.568		
Total	8	30.199			

Model Summary

S	R-sq	R-sq(adj)	R-sq(pred)
2.13734	9.24%	0.00%	0.00%

Means

Factor	N	Mean	StDev	95% CI
L-1000-LIN	3	3.88	1.88	(0.86, 6.90)
L-1000-NH	3	3.88	1.76	(0.86, 6.90)
L-1000-PE	3	5.06	2.65	(2.04, 8.08)

Pooled StDev = 2.13734

Tukey Pairwise Comparisons

Grouping Information Using the Tukey Method and 95% Confidence

Factor	N	Mean	Grouping
L-1000-PE	3	5.06	A
L-1000-NH	3	3.88	A
L-1000-LIN	3	3.88	A

Means that do not share a letter are significantly different.

Figure D.4: ANOVA and Tukey comparisons of lateral tibial cartilage contact pressure for 1000N load applied at 0 degree flexion angle.

One-way ANOVA: M-30-LIN, M-30-NH, M-30-PE

Method

Null hypothesis	All means are equal
Alternative hypothesis	Not all means are equal
Significance level	α = 0.05

Equal variances were assumed for the analysis.

Factor Information

Factor	Levels	Values
Factor	3	M-30-LIN, M-30-NH, M-30-PE

Analysis of Variance

Source	DF	Adj SS	Adj MS	F-Value	P-Value
Factor	2	9.947	4.973	2.10	0.204
Error	6	14.227	2.371		
Total	8	24.173			

Model Summary

S	R-sq	R-sq(adj)	R-sq(pred)
1.53984	41.15%	21.53%	0.00%

Means

Factor	N	Mean	StDev	95% CI
M-30-LIN	3	7.065	0.995	(4.890, 9.241)
M-30-NH	3	7.046	0.967	(4.870, 9.221)
M-30-PE	3	9.29	2.28	(7.11, 11.46)

Pooled StDev = 1.53984

Tukey Pairwise Comparisons

Grouping Information Using the Tukey Method and 95% Confidence

Factor	N	Mean	Grouping
M-30-PE	3	9.29	A
M-30-LIN	3	7.065	A
M-30-NH	3	7.046	A

Means that do not share a letter are significantly different.

Figure D.5: ANOVA and Tukey comparisons of medial tibial cartilage contact pressure for 1000N load applied at 30 degree flexion angle.

One-way ANOVA: L-30-LIN, L-30-NH, L-30-PE

Method

Null hypothesis	All means are equal
Alternative hypothesis	Not all means are equal
Significance level	α = 0.05

Equal variances were assumed for the analysis.

Factor Information

Factor	Levels	Values
Factor	3	L-30-LIN, L-30-NH, L-30-PE

Analysis of Variance

Source	DF	Adj SS	Adj MS	F-Value	P-Value
Factor	2	19.33	9.663	0.62	0.569
Error	6	93.36	15.560		
Total	8	112.68			

Model Summary

S	R-sq	R-sq(adj)	R-sq(pred)
3.94460	17.15%	0.00%	0.00%

Means

Factor	N	Mean	StDev	95% CI
L-30-LIN	3	7.42	3.42	(1.85, 13.00)
L-30-NH	3	7.37	3.42	(1.80, 12.94)
L-30-PE	3	10.50	4.83	(4.93, 16.08)

Pooled StDev = 3.94460

Tukey Pairwise Comparisons

Grouping Information Using the Tukey Method and 95% Confidence

Factor	N	Mean	Grouping
L-30-PE	3	10.50	A
L-30-LIN	3	7.42	A
L-30-NH	3	7.37	A

Means that do not share a letter are significantly different.

Figure D.6: ANOVA and Tukey comparisons of lateral tibial cartilage contact pressure for 1000N load applied at 30 degree flexion angle.

Appendix E: Extended Model Development Methods

Model Development Summary

An overview of the model development process used in this study and examples of intermediate products is shown graphically in Figure E.1.

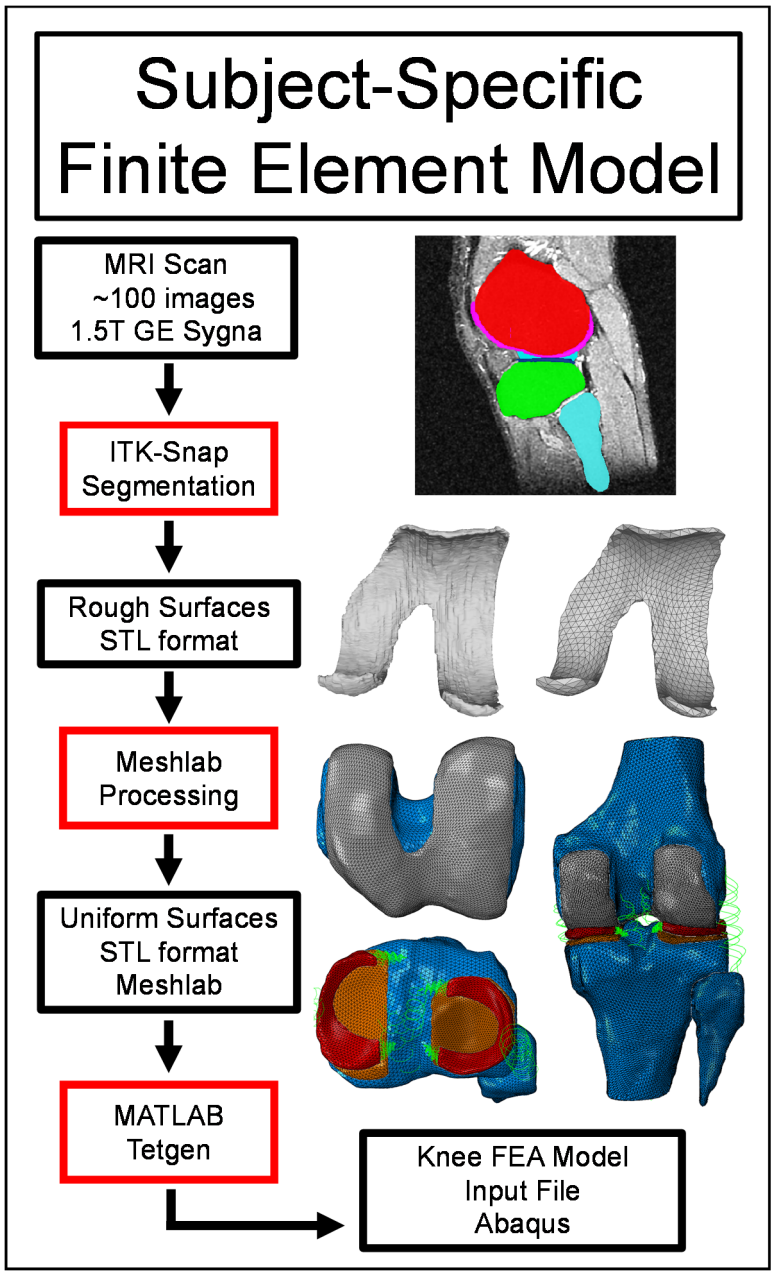

Figure E.1: Overview of the subject-specific modeling process showing software programs and examples of intermediate products.

Segmentation

The boundaries of each tissue within the MRIs of the TF joint were identified and manually outlined, a process referred to as segmentation, using an open-source program, ITK-SNAP [65]. Outlining the boundaries of each tissue was performed using the following order for all models: femoral cartilage, tibial cartilage, menisci, and bone. Following the specified order of tissues was a good way to ensure the cartilage geometry was accurately outlined. The majority of time and attention was given to outlining the cartilage and menisci, the soft tissues that affect the outcome of this analysis. Outlining bone geometry away from the bone-cartilage interface was not highly important to the analysis being performed in this study. The MRI scan settings used did not produce sufficient images of the ligaments to create a 3-D body. The ligament insertion sites were identified on the surfaces of the femur, tibia, and fibula, and allowed for appropriate placement of the ligament spring elements. An example of the completed segmentation is shown in Figure E.2.

Defining each tissue boundary in all sagittal plane views allowed ITK-SNAP to create a closed or nearly-closed three dimension surface. Exporting each of the generated 3-D surfaces as an individual STL file increased the ability to process each body's surface independently and achieved the highest quality knee assembly.

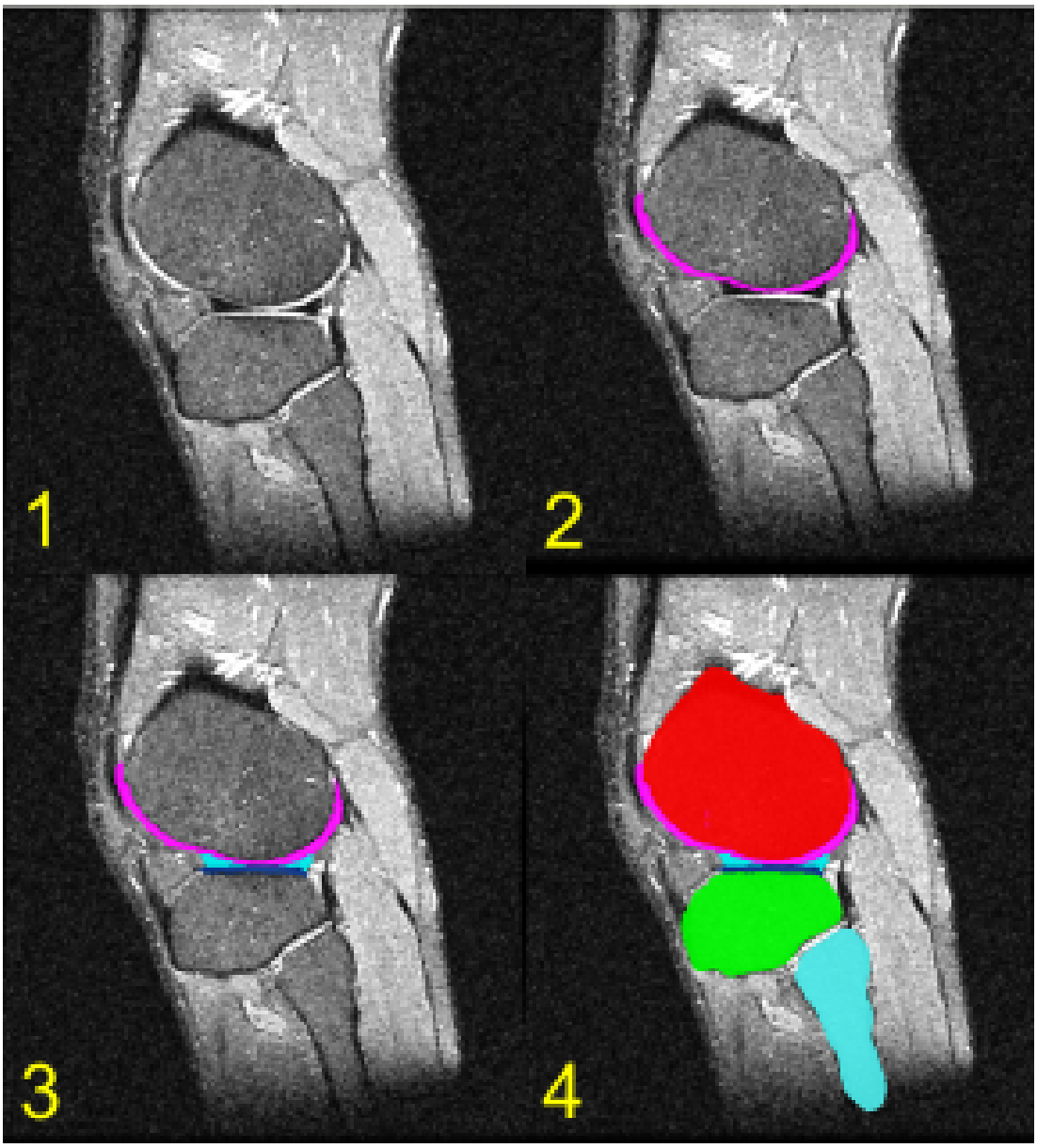

Figure E.2: Femur (red), Tibia (green), Fibula (teal), femoral cartilage (pink), tibial cartilage (blue), menisci (aqua), were outlined in ITK-SNAP.

Three-Dimensional Surface Processing

The three-dimensional surfaces for each body exported from ITK-SNAP contained features which were not sufficiently well-conditioned to allow for analyses such as holes, tunnels, bumps, and “staircase” artifact. Staircase artifact results from using a limited number of 2-D slices to build a 3-D model.

For our models built with between 80-110 2-D slices the discontinuities between outlined boundaries were challenging to fill and resulted in unrealistic 3-D surfaces. In addition the image resolution and user error associated with manually outlined tissue boundaries generated surfaces that were not expected to be smooth. As such it was necessary to create 3-D surfaces that were watertight, sufficiently smooth, had a suitable mesh density, and had elements with approximately equal edge lengths through surface processing.

A number of so-called “filters” were applied in the open-source mesh processing tool MeshLab. Within MeshLab, cleaning, smoothing, reconstruction, face reduction, and isoparameterization filters created a high quality surface mesh. Intermediate products of each filter are shown in Figure E.3. Isoparameterization is a process by which an abstract domain mesh is calculated, and remeshing allows for efficient and uniform mesh refinement. Several examples of an isoparameterized femoral cartilage mesh with different edge lengths is shown in Figure E.4. Mesh edge lengths were measured using a custom-written MATLAB script.

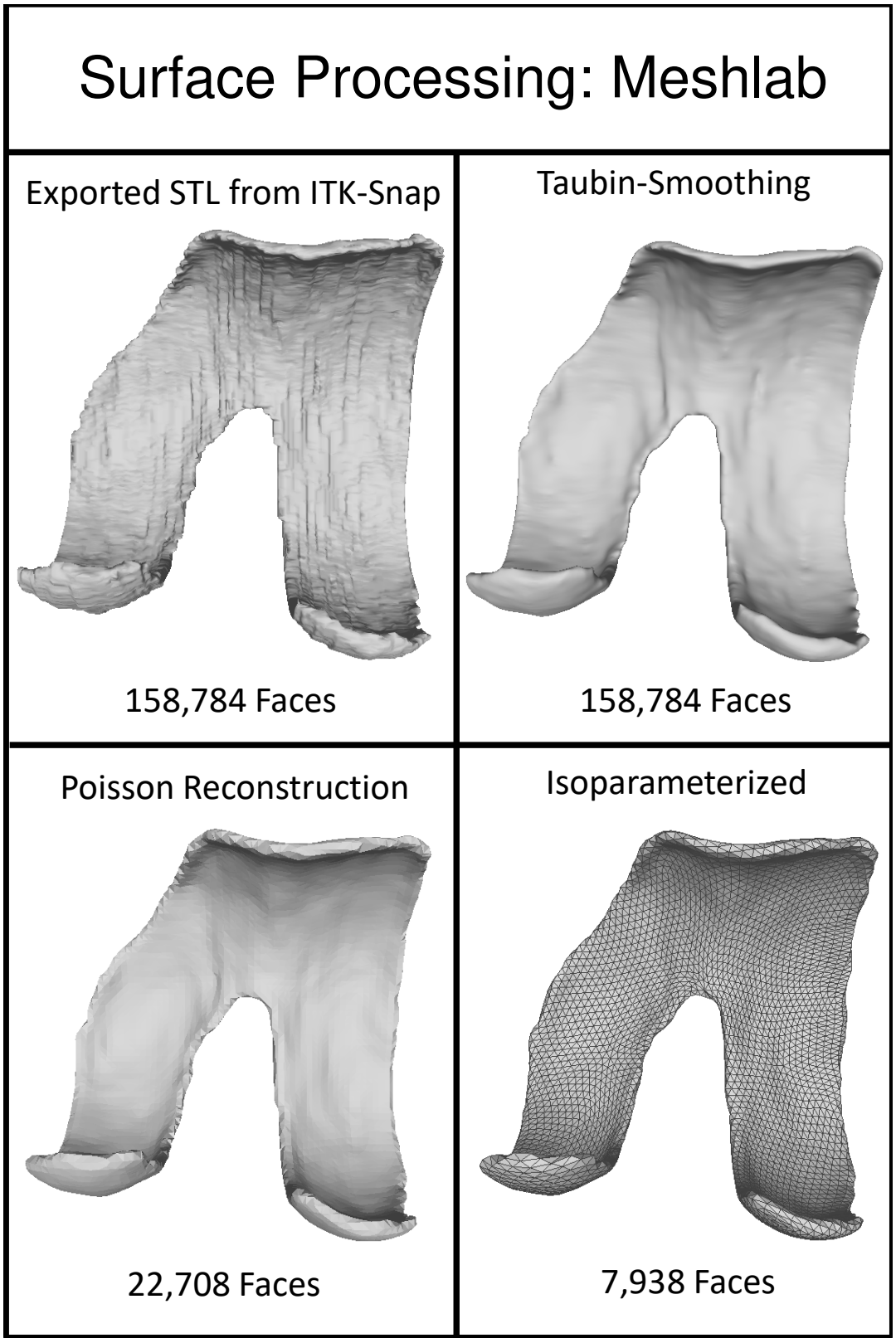

Figure E.3: Surface processing overview with femoral cartilage as example.

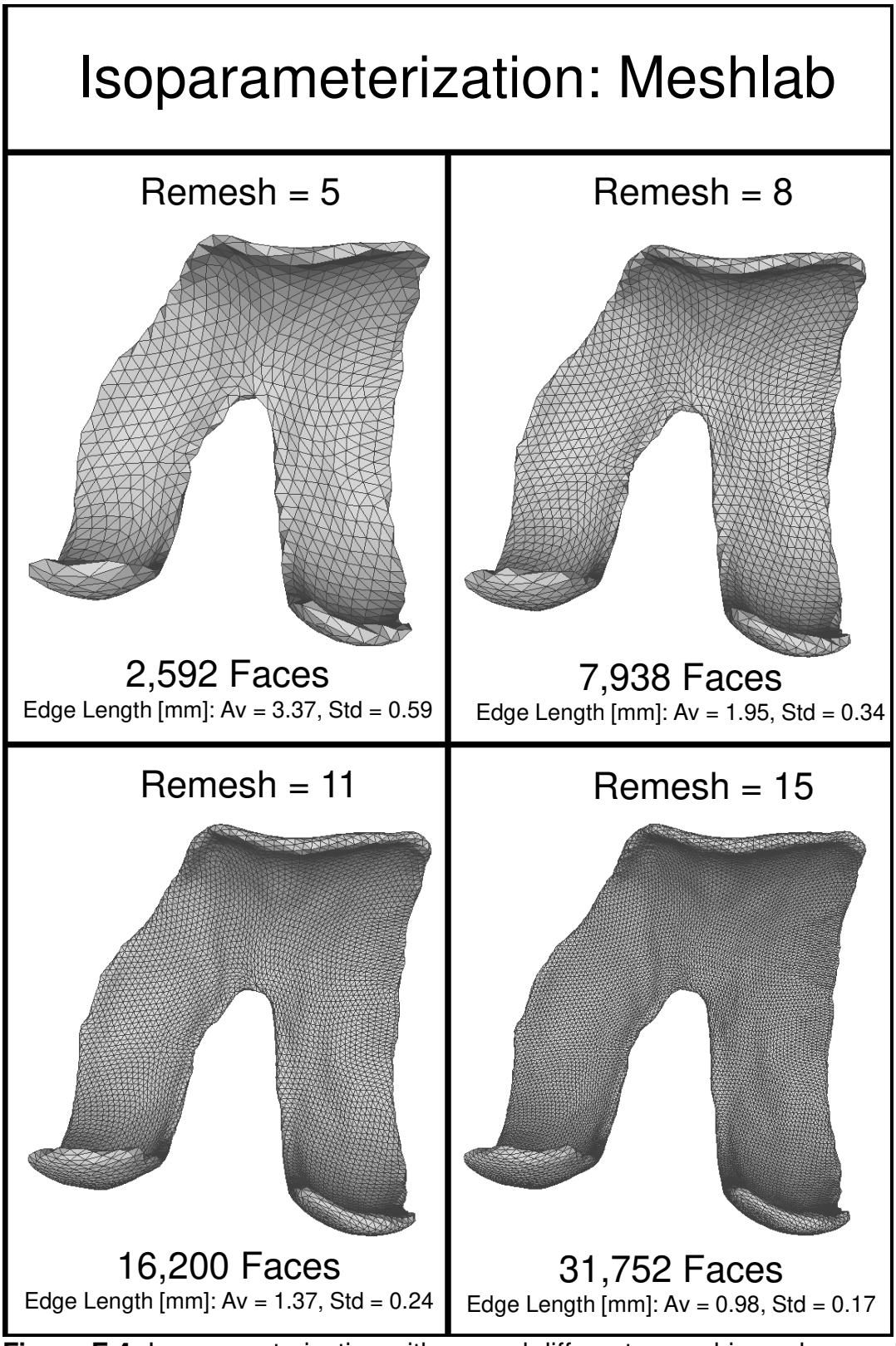

Figure E.4: Isoparameterization with several different remeshing values and the edge lengths for each femoral cartilage surface mesh STL.

Tetrahedral Element Mesh

The cartilage and menisci finite element meshes were made entirely of quadratic 10-noded tetrahedral elements. The quality of the tetrahedral element in the cartilage and menisci was directly related to the performance of the finite element model and as such it was necessary to create the highest quality mesh possible. In addition to element quality measures, it was necessary that element counts be within a reasonable range to preserve reasonable computational costs. Following the three-dimensional surface processing and isoparameterization, each remeshed STL surface for the cartilages and menisci was used to generate a set of tetrahedral meshes shown in Table E.1. Each group of tetrahedral meshes was imported as a separate part into Abaqus using a custom MATLAB script in order to find appropriate mesh quality measures using the Abaqus verify mesh feature. For generation of the computational mesh, the Delaunay tetrahedralization scheme TetGen was used [45]. TetGen input strings 'pq4/10Aa10VO7' for femoral cartilage and 'pq5/15Aa10VO7' for tibial cartilages and menisci were specified. TetGen was implemented as part of the Geometry and Image-Based Bioengineering add-On (GIBBON) [67] for MATLAB.

Table E.1: Measurements of several medial tibial cartilage meshes for the purpose of determining the most suitable meshes for FEA.

Edge Length Average *[mm]*	Edge Length Std. Dev *[mm]*	10-noded Tetrahedral Elements *[10^3]*	Mesh Analysis Warning *[Abaqus Verify]*	Total Number Nodes *[10^3]*	Total Number DOF *[10^3]*
1.94	0.33	1	8	3	9
1.56	0.27	3	8	5	15
1.31	0.22	4	22	8	23
1.12	0.19	6	31	11	34
0.98	0.17	9	23	16	48
0.88	0.15	12	30	21	64
0.79	0.14	17	41	29	86
0.72	0.12	21	54	36	108
0.66	0.11	26	50	44	132
0.61	0.11	34	81	56	167
0.56	0.10	39	86	65	194

Assembly Development

The cartilages, menisci, and bones comprised the 8 meshed parts included in the Abaqus assembly. In addition to the parts, a number of settings and features were created and defined in order to create a working finite element model.

In this study the knee coordinate system was created by a flexion/extension axis passing through the medial and lateral femoral condyles and an internal/external rotation axis passing through the femur. Selecting a local coordinate system for the femur and tibia was necessary in order to accurately apply knee joint loading cases Although each MRI scan was performed with approximately the same orientation, there was no special attention given to the subject's knee position in regard to the MRI coordinate system. The process of registration, identifying subject-specific anatomical

features to create a local coordinate system from a subject-specific model, required accurately identifying the femoral condyles for our knee model. Model registration is a current research topic under much development because it is highly important and poorly understood in various computational image-based modeling processes. The femoral condyles in our models were plateaued and as such it was challenging to select a single reference point to identify the femoral condyle. The local coordinate system knee-axis was visualized within Abaqus and was adjusted as necessary, with modifications made using visual judgement.

The reference points for the femur, tibia, and fibula were also selected. The femur reference point was defined as the midpoint between the medial and lateral condyles. Compressive forces and flexion rotation angles for each loading case were applied to the femur reference point and as such its location was expected to affect results. The tibia reference point was defined on the distal end, the placement of which was not nearly as important as the femur reference point. The fibula reference point was selected as the most superior node in the mesh because its location was also of little or no consequence.

Output Variable

It was necessary to specify outputs of interests and suppress unwanted variables in order to decrease memory usage. The essential output variables were the displacement (U) and contact pressure (CPRESS). The displacements were useful to visualize the loading case with an applied rotation of 30 degrees. Cartilage contact pressure was compared to experimental results by other

researchers using digital pressure sensors such as tek-scan[47]. In addition, the nature of the knee cartilage being modeled as a homogenous material made finding depth dependent stresses and strains undesirable and unlikely to produce meaningful results. Other studies have also reported the contact area, CAREA, as part of their results [12, 20]. Contact area is also a useful output variable to include but it was not reported in this thesis.

Maximum contact pressures were determined by averaging multiple nodes surrounding the single-node with the maximum value. Possible uniform averages to perform on the 10-noded tetrahedral elements were the 7 and 19 node averages. The 19 node average has an approximate area of 1 mm^2 which was reasonable to compare with digital pressure sensors used for validation studies [47]. It was useful to determine the maximum contact pressure for both the lateral and medial sides, and as such an average was performed for each surface.

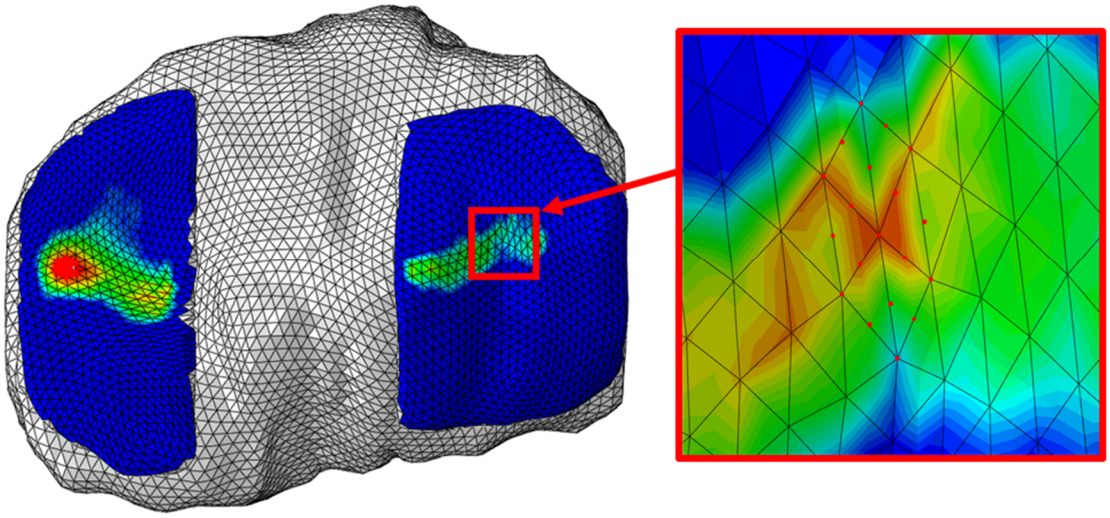

Figure E.5: Finding Maximum contact pressure for the lateral compartment by averaging all nodes within 6 element faces.

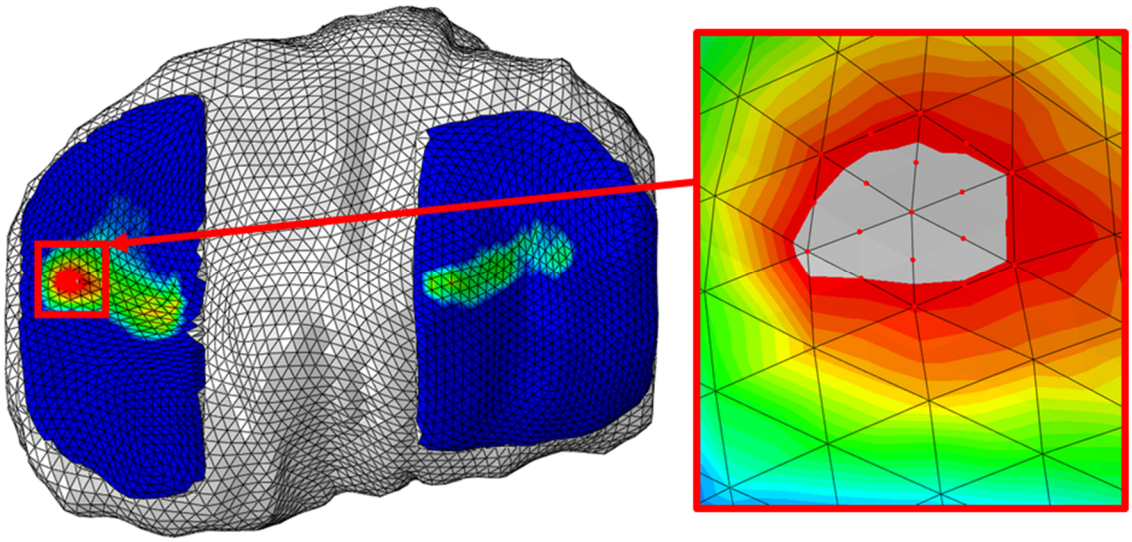

Figure E.6: Finding Maximum contact pressure for the medial compartment by averaging all nodes within 6 element faces.

Non-default Solver Settings

Several changes to the default model setting were found to be necessary in order to efficiently and accurately obtain results. One such unexpectedly important setting was the unsymmetric matrix storage. It was observed that unsymmetric matrix storage was needed to solve solution increments for every knee model. By default Abaqus uses symmetric matrix storage and solution, as this is expected to work for nearly all meshes. The ligament and meniscal horn attachment springs were the most likely reason for unsymmetric matrix storage and solution to be consistently necessary to solve the model.

The pseudo-time incrementation was adjusted for efficient model solution. For the 1st step, the time increment was set to an initial value of 1e-2. The number of equilibrium iterations attempted was increased to 50. The number of time increment cutbacks allowed was typically 5, although there were times to

increase this number if you specify small time increments beyond which cutbacks are not desirable and useful.

Non-linear geometry solver settings were specified in both analysis steps of the model. Non-linear geometry recalculates the stress at each increment based on the deformed geometry as opposed to a linear geometry setting which performs analyses on the undeformed geometry for all time increments. Deformations expected in analyses were classified as being greater than infinitesimal but far away from what is typically considered large-deformation.

Finalized Knee Geometry

A convergence study of the model was conducted by refining the cartilaginous bodies to different levels in MeshLab as detailed in [68]. The results of the convergence study performed on Model 1 indicated that the contact pressure at several locations was considered sufficiently converged. There was a significant time cost associated with developing models with different amounts of mesh refinement, and as such only a convergence study on subject 1 was performed. It should be noted that the model convergence was performed using a LIN cartilage material model. Given the scope and aims of this study and the time investment of developing a finite element model it was not feasible to perform a thorough convergence study on all of the models. Model 2 and Model 3 were selected to most nearly match the element numbers of the converged Model 1. The number of elements of each body for the finalized knee models of subjects 1, 2, and 3 are given in Table E.2. The mesh appearances of each body

for all subjects is shown in Figures E.7-10. The completed knee assembly for each subject is shown in Figures E.11-13.

Table E.2: Number of elements for each subject-specific model.

Body	Subject 1 Elements [10^3]	Subject 2 Elements [10^3]	Subject 3 Elements [10^3]
Femoral Cartilage	38	44	30
Femur	14	13	11
Lateral Tibial Cartilage	12	7	7
Medial Tibial Cartilage	5	4	6
Tibia	13	13	14
Lateral Meniscus	5	7	7
Medial Meniscus	5	10	7
Fibula	7	8	3
Total	99	107	85

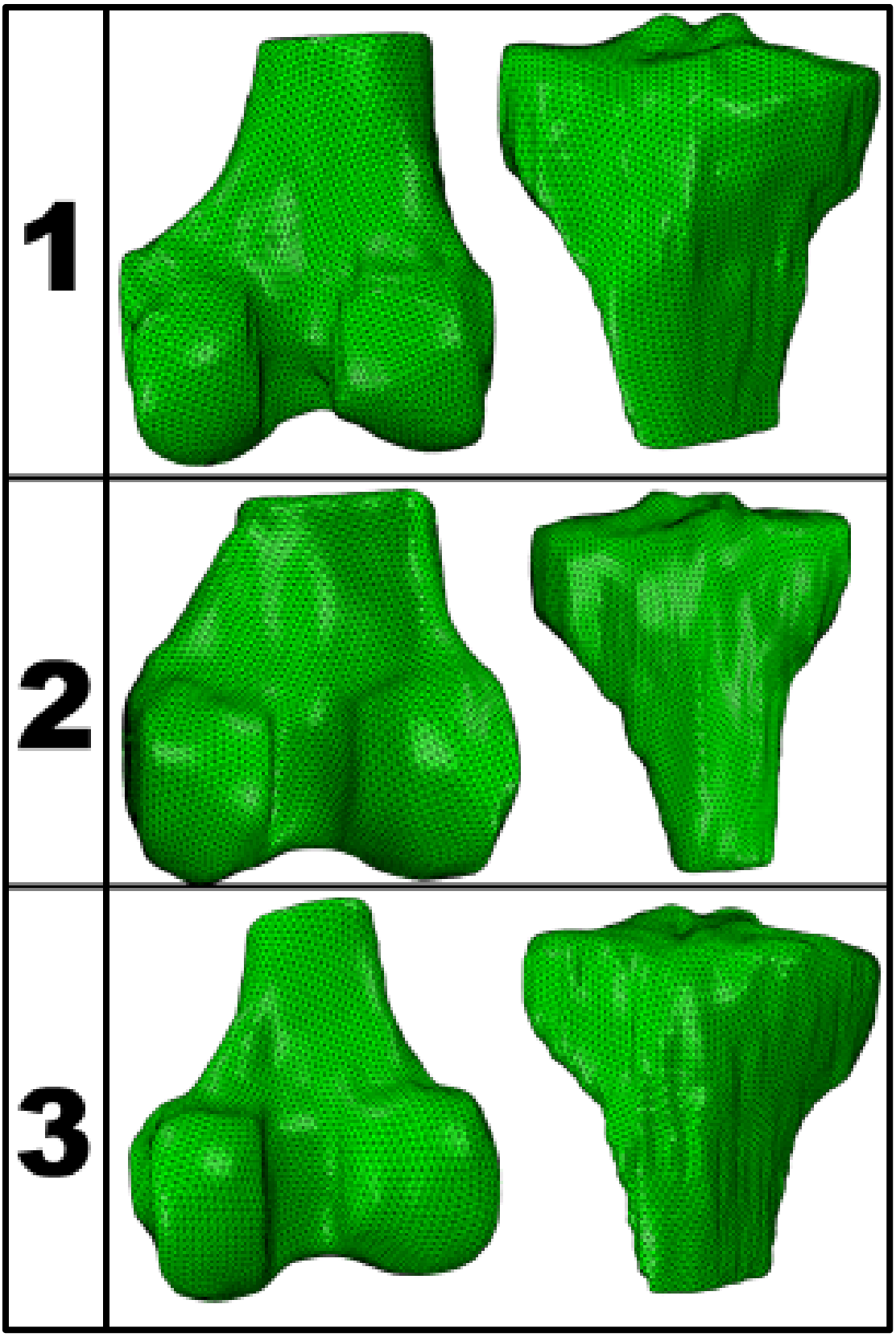

Figure E.7: Meshes of the femur and tibia for all subjects.

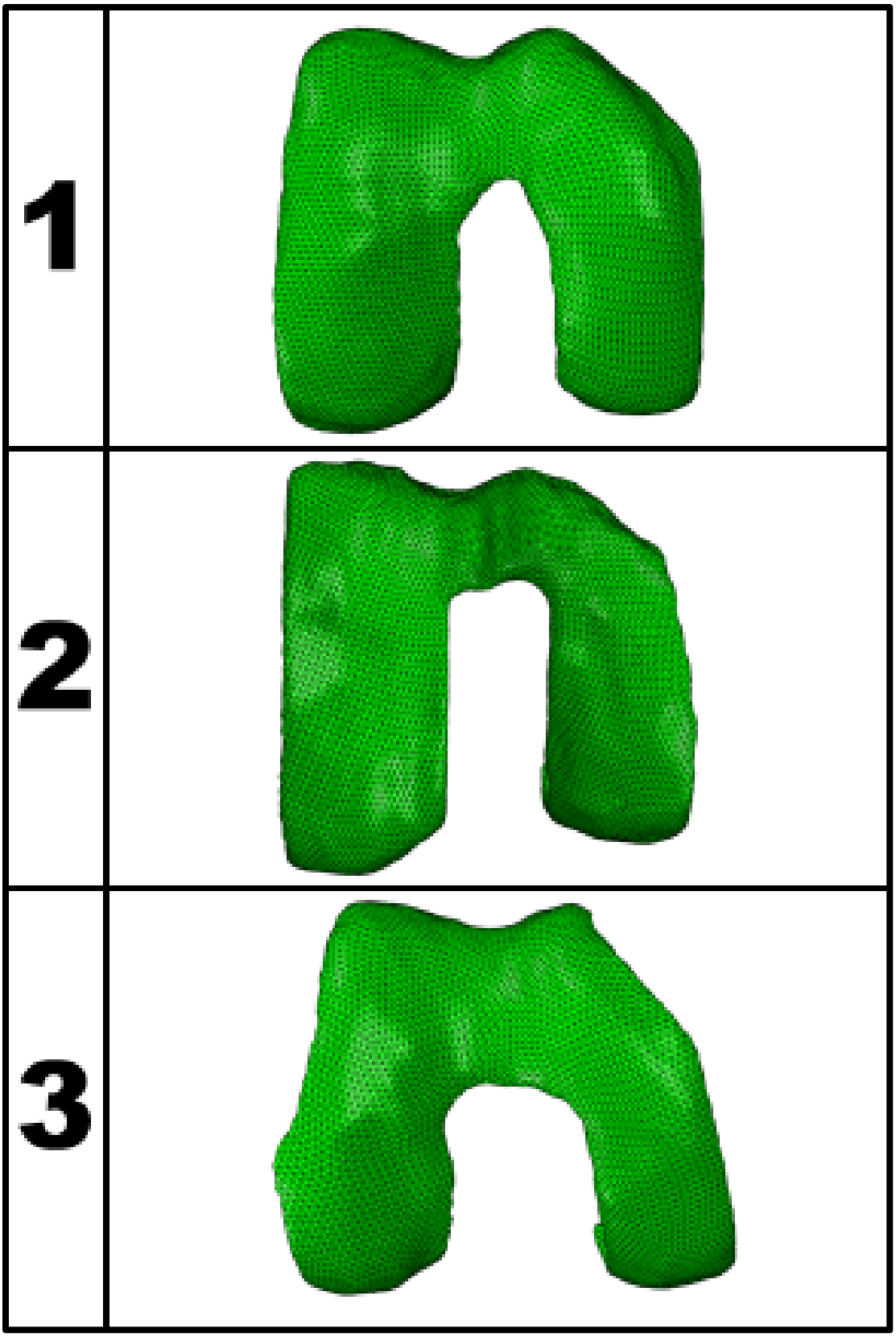

Figure E.8: Meshes of the femoral cartilage for all subjects.

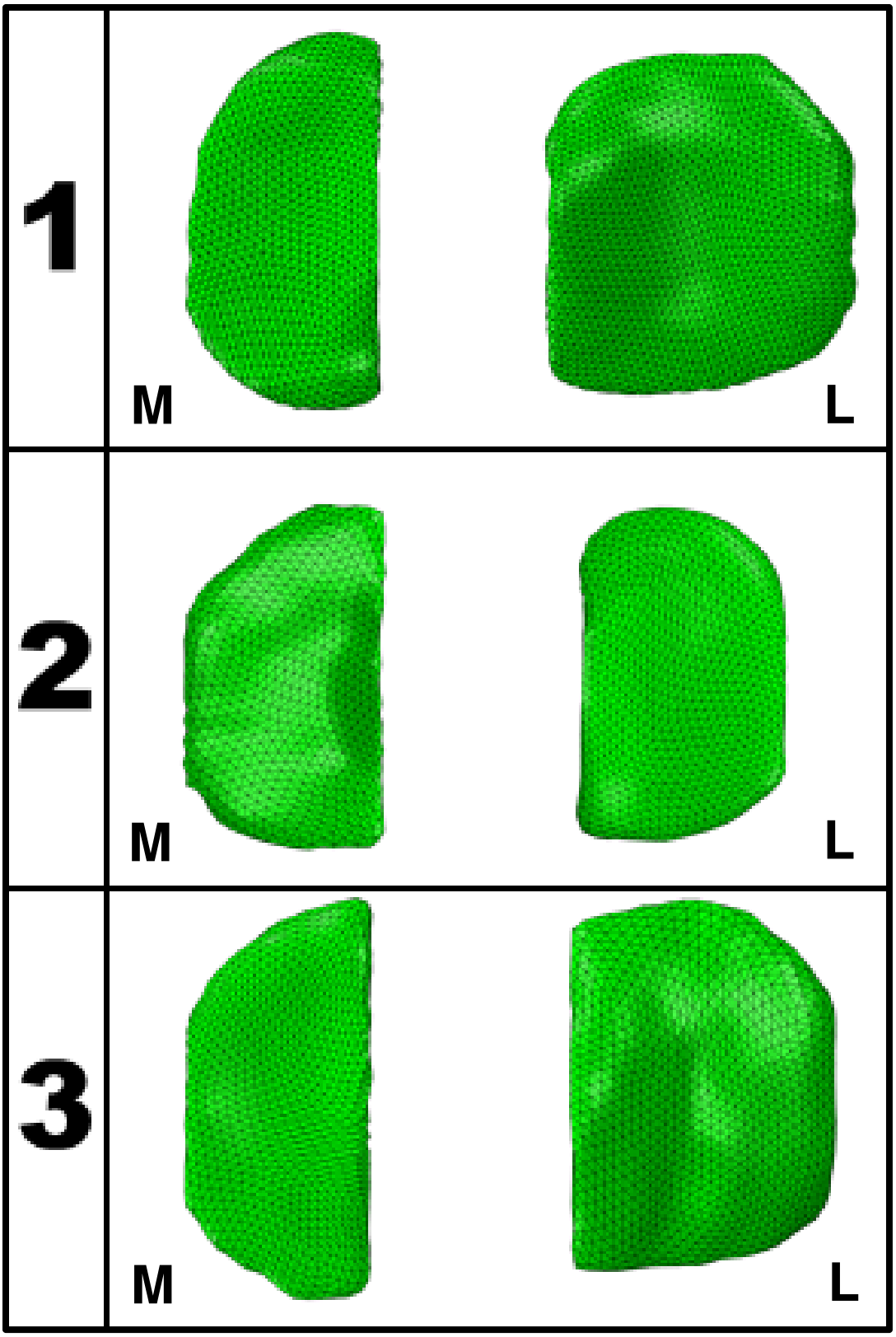

Figure E.9: Meshes of the medial (M) and lateral (L) tibial cartilages for all subjects.

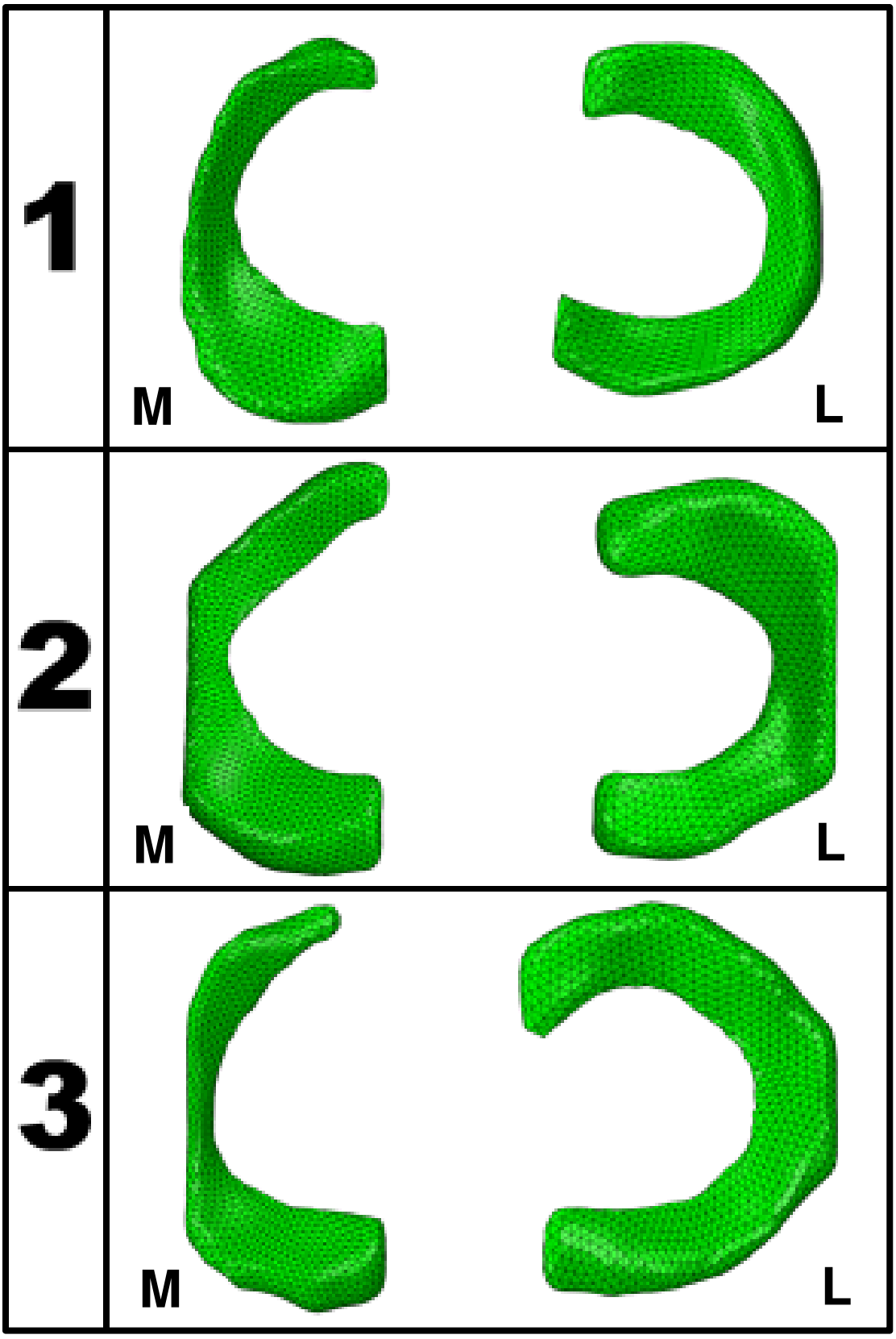

Figure E.10: Meshes of the medial (M) and lateral (L) menisci for all subjects.

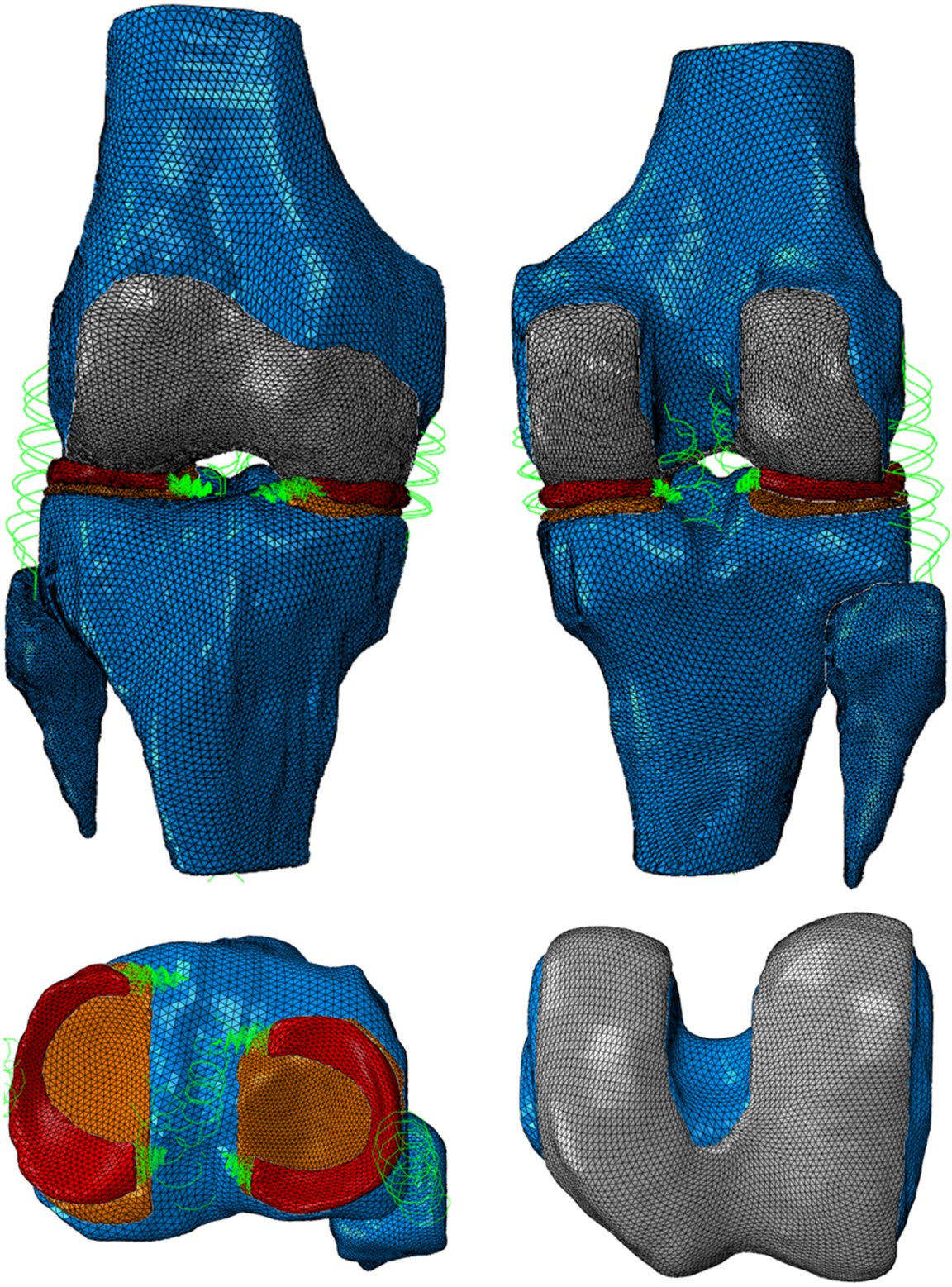

Figure E.11: Subject 1 Knee Mesh Assembly (Right Knee).

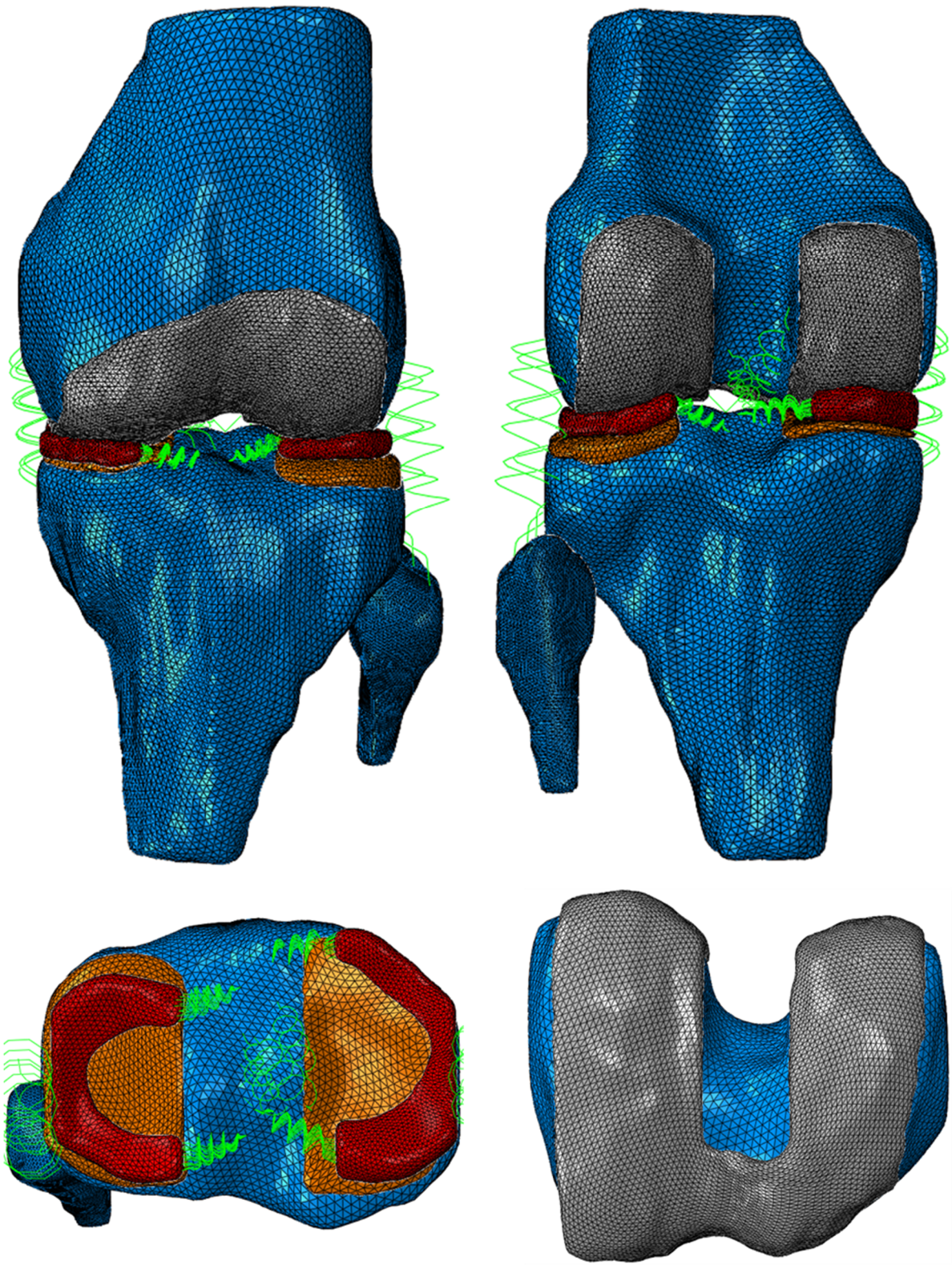

Figure E.12: Subject 2 Knee Mesh Assembly (Left Knee).

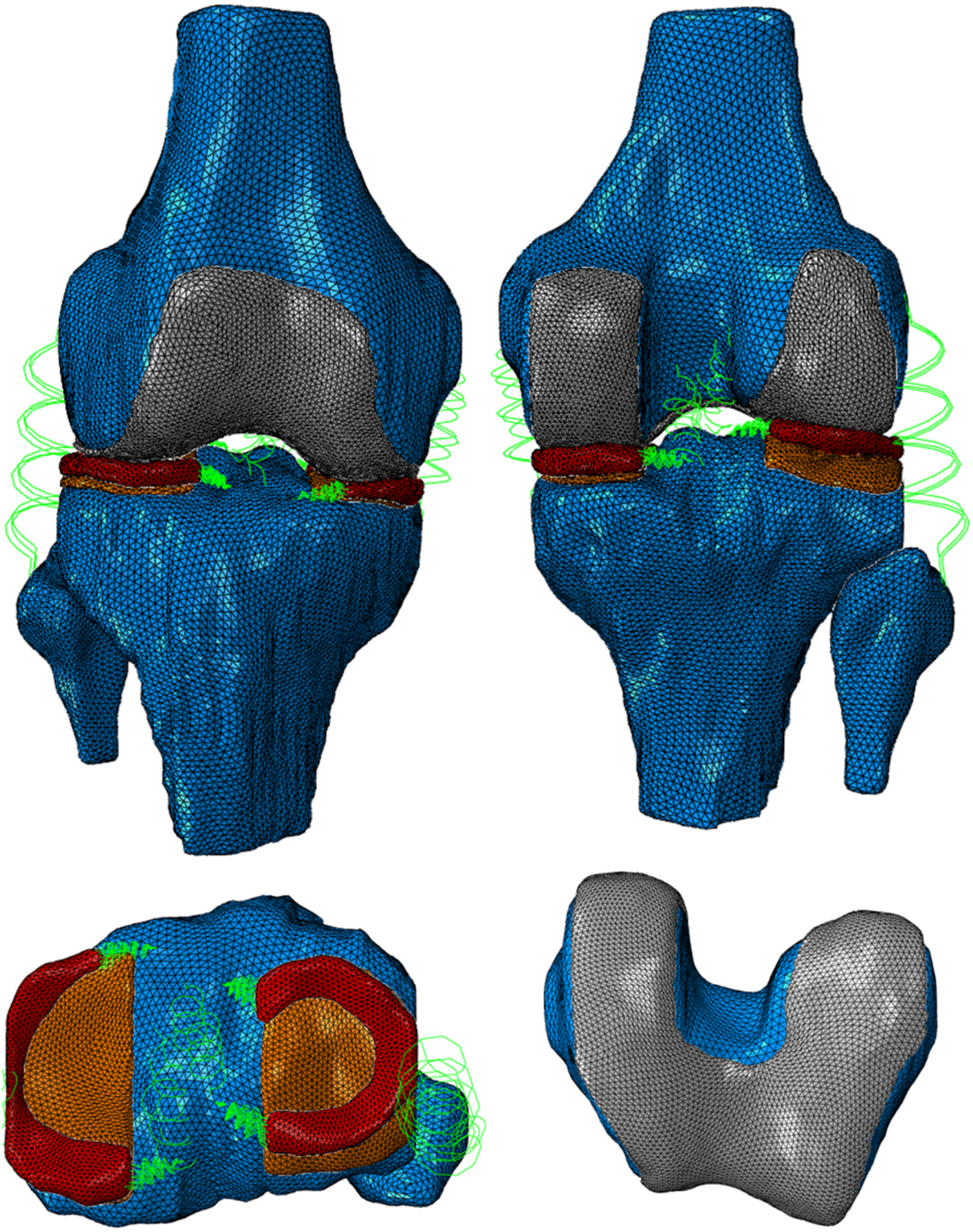

Figure E.13: Subject 3 Knee Mesh Assembly (Right Knee).